Final Report

PARTICLE-DETECTOR STUDIES ON LUNAR ORBITAL MISSIONS

NASA Contract NAS 9-9895

30 June 1969 to 30 June 1970

Principal Investigator —
Professor K.A. Anderson

SSL Series 11, Issue 84

14 December 1970

UNIVERSITY OF CALIFORNIA, BERKELEY

CR-114858
C. 1

Space Sciences Laboratory Series 11, Issue 84

Final Report

PARTICLE DETECTOR STUDIES ON LUNAR ORBITAL MISSIONS

NASA Contract NAS 9-9895

(30 June 1969 to 30 June 1970)

Prepared by

Space Sciences Laboratory
University of California
Berkeley, California 94720

Principal Investigator Professor K. A. Anderson

for

Manned Spacecraft Center
Houston, Texas 77058

14 December 1970

TABLE OF CONTENTS

ABSTRACT

A set of electrostatic analyzers and solid state detectors were tested to determine their suitability for use on Apollo lunar orbital missions. The electrostatic analyzers were required to have high sensitivity to the low fluxes of energetic solar electrons while at the same time they were required to reject large fluxes of solar ultraviolet. To obtain high electron sensitivity, five funnel-mouthed continuous channel electron multipliers were used in parallel which gave a total geometric factor of 0.63 cm^2 sr keV. To reject ultraviolet the electrode plates were serrated and coated with gold black. This procedure reduced ultraviolet intensity reaching the detectors by 12 orders of magnitude. The solid state detectors were required to have low electron energy threshold, high resolution and low noise counting rate. Results show that a lithium drift detector can be used for electrons with energies as low as 5.9 keV.

LIST OF TABLES

LIST OF ILLUSTRATIONS

I. PURPOSE

The purpose of this study was to develop an array of charged particle detectors suitable for Apollo lunar orbital missions. The proposed array consists of four electrostatic analyzers and two solid state detectors. The electrostatic analyzers were designed to measure electron fluxes at four different energies between 0.5 keV and 15 keV. The solid state detectors were designed to measure electron fluxes between 20 keV and 320 keV and proton fluxes between 50 keV and 2 MeV.

II. THE ELECTROSTATIC ANALYZERS

Each electrostatic analyzer consists of two concentric hemispherical electrode plates with a positive potential applied to the inner plate. Electrons of the proper energy that enter the plates are deflected 180° into a continuous channel electron multiplier (CCEM). The proper electron energy is determined by the radii of the plates and the applied voltage. Table 1 is a summary of the characteristics of the four analyzers proposed for lunar orbital missions. The third analyzer A3 has two CCEM's of different sensitive areas to provide a wider dynamic range. Thus A3 has two detector outputs C_3 and C_4. Figure 1 is a schematic section of one of the analyzers.

Particle Response

The response of an electrostatic analyzer to incident particles depends both on particle energy and incident angle. The response can be defined as the ratio of the observed count rate, CR(counts/sec) in the analyzer to the incident flux, J(particles/cm^{2}sec), of particles at a given energy, E(keV), and incident angle, α. If we integrate over all incident angles we obtain the geometric factor, g(E)(cm^2 sr), as a function of energy. The response of each of the proposed analyzers was calculated numerically and tabulated against particle energy and incidence angle to form a transmission matrix. The transmission matrices for each analyzer are shown in Tables 2, 3, 4, 5 and 6. The method for calculating the transmission matrix is given in Appendix I. The particle response of detector C_5 was verified experimentally in the laboratory. The results of this test are presented in Figure 2. The results indicate that the beam is deflected by 4^o before entering the analyzer. This is probably due to fringing of the electric field between the plates at the entrance to the analyzer.

Ultraviolet Response

During lunar orbital missions the analyzers will sometimes look directly at the sun, which is a potent source of ultraviolet radiation. Since CCEM's are sensitive to ultraviolet we had to develop a means of preventing ultraviolet from reaching the CCEM's. A low background count rate due to solar ultraviolet is required to obtain the minimum detectable particle flux thresholds required. Table 7 summarizes the background level requirements for the analyzers. Since the flux of ultraviolet from the sun is about 10^{12} photons/cm^2 sec, the design goal for C_5 required reduction in ultraviolet intensity by a factor of 10^{14}. To test for ultraviolet rejection in the laboratory we built a hydrogen arc lamp The arc lamp was calibrated with a gold diode and found to have an intensity of more than 10^{12} photons/cm^2 sec of hydrogen Lyman-α ultraviolet.

To prevent ultraviolet from reaching the detectors the analyzers were sealed such that the only way for radiation to reach the detectors was to scatter between the hemispherical plates. The plates were coated with gold black to absorb the ultraviolet. Gold black is formed by evaporating gold in 1 mm Hg pressure. The evaporated gold condenses into spheriods of approximately 1 micron diameter and are deposited on the surface. A thick coating of spheriods acts as a radiation trap. The total integrated reflectance of a gold black surface to hydrogen Lyman-α is 1.9%.

A C_5 detector with gold blacked plates showed 11 counts/sec when 10^{12} photon/cm^2 was normally incident on the analyzer. Since on a spinning satellite an analyzer would be looking at the sun only a small fraction of the time, the background count rate would be 1.1 counts/sec in flight.

To further reduce ultraviolet background we seriated the outer hemispherical plate. The serrations were designed to scatter light back out the entrance to the analyzer (Figure 3). We tried a C_5 detector with 11° serrated gold blacked plates and obtained a count rate of 4 counts/sec when 10^{12} photons/cm^2 sec was normally incident on the analyzer. Serrations of 35° angle were found to be superior to 11° serrations. In this case the C_5 detector showed 0.4 counts/sec with normally incident 10^{12} photons/cm^2 sec.

At angle greater than normal incidence the background rate is higher. For instance for the C_4 detector at 18° from normal the background level is 50 counts/sec as compared to 3.2 counts/sec at normal incidence of 10^{12} photons/cm^2 sec. In flight the ultraviolet background can be reduced by utilizing a sunshade to prevent large incident angles. Figure 4 illustrates the effect of a sunshade. A factor of 12 improvement can be obtained by a sunshade 2 inches long. Table 8 summarizes the expected background count rates due to solar ultraviolet in each of the analyzers.

Cosmic Rays

Another source of background count rate in the detectors is cosmic rays. To eliminate cosmic ray background detectors C_4 and C_5 were surrounded by a plastic phosphor scintillator and a photomultiplier tube. Thus when a cosmic ray passes through a CCEM detector it also causes a flash in the scintillator and the count in the CCEM is then rejected. The particles that the analyzer selects are much less energetic than cosmic rays and cause counts only in the CCEM. To test the ability of the scintillator to reject cosmic rays we used the test set up shown in Figure 5. Scintillators A and B are arranged such that when there is a coincidence in A and B a cosmic ray must have passed through the scintillator shield C that we want to test. If C were 100% efficient then whenever there is a coincidence between A and B then there should be a pulse from C. In the test we found that the shield surrounding the C_5 detector was 63% efficient.

Detector Lifetime

The gain of CCEM's is known to decrease with lifetime. We tested two Bendix type 4219 "Spiraltrons" that we propose to use with the analyzers. The results shown in Figure 6 show that the gain decreased from over 10^8 to 1.2×10^6 at 8×10^9 total accumulated counts and count rate of 6×10^4 counts/sec and stayed at that level to the end of the test at 2×10^{10} total counts. The test also showed that the gain recovered considerably whenever the source was turned off. We also found that the gain was greater at lower count rate. At the end of the lifetime test we operated the CCEM at lower count rate (3.2×10^3 counts/sec compared to 6×10^4 counts/sec) and found the gain increased from 1.2×10^6 to 4×10^7.

III. SOLID STATE DETECTORS

The two solid state sensors are identical except for a thin foil (about 500 μ gm/cm^2) over one detector. Each detector consists of two back to back semiconductor detectors of 25 and 50 cm^2 area. The front detector has an electron threshold of 20 keV at room temperature. Protons from 50 keV up to 6.0 MeV can also be detected by this detector.

Particle Response

The foil produces a drastic shift in a proton spectrum but a small shift in an electron spectrum. Thus it is possible to sort out proton from electron spectra in a statistical way. The key to making a foil system from which false conclusions cannot be drawn is that the thickness of the solid state crystal is the range of a 300 keV electron and the thickness of the foil is the range of a proton of the same energy. In the open detector, electrons in the energy range 25 to 300 keV and protons in the energy range 50 to 300 keV are detected together and cannot be separated but protons of greater energy than 300 keV are detected unambiguously. In the foil detector, electrons in the energy range 25 to 300 keV are detected with protons in the range 300 to 450 keV. But the measurement of greater than 300 keV protons from the open detector allows us to subtract the proton flux from the electron measurement in the foil detector.

Detector Performance

The solid state detector system has been investigated to determine the following properties

1. The maximum electron energy resolution that can be achieved.
2. The lowest energy threshold that can be measured, theoretically as well as practically.
3. The effect of operating temperature of the detector telescope in the spacecraft on performance.
4. The maximum counting rate without pulse height distortion.
5. The kind of electronic circuitry required to obtain an optimum performance of the detector.

The amount of charge generated in a solid state detector by an incident electron is proportional to the electron energy. Noise is generated continuously in a solid state detector by random fluctuations in the leakage current. Any charge pulse due to an incident electron is superimposed on the noise. Thus, the pulses from electrons of a given energy have different pulse heights depending on the noise.

A pulse height spectrum is obtained by plotting number of pulses accumulated against pulse height. If there were no noise the pulse height spectrum from electrons of a given energy would be a narrow line at a single pulse height. With noise the spectrum becomes a broad line. The amount of broadening or resolution is measured by the difference of pulse height values (full width) at one half the maximum number of counts accumulated, and is usually given in units of energy since the pulse heights are calibrated against energy.

The lowest energy electron that can be detected is determined by the background counting rate due to noise that can be tolerated. If the minimum electron energy threshold is so low that its pulse height is nearly the same as the noise due to leakage current fluctuations then there is a large noise counting rate. If one wants to measure low fluxes of electrons then the electron energy threshold must be raised to a point where the background counting rate due to noise is tolerable.

It is desireable to have a system with low noise since both resolution and energy threshold can be improved. In order to understand how minimum noise can be achieved, a brief description of the theory of noise generation in a solid state detector and electronic circuitry is required.

Current Noise. When voltage is applied on the solid state detector, it generates shot noise due to random electron leakage current fluctuations. We are interested in the average charge deposit from noise. First we calculate the average of the square of the variations of current over a certain time

$$\overline{i_b}^2 = \overline{\left(I_b - I_{dc}\right)}^2 = \frac{1}{T_1} \int^{t_1} \left(I_b - I_{dc}\right)^2 \; dt$$

where

i_b = spontaneous current generated by one electron

I_b = instantaneous current composed of superpositions of a number of electron deposits

I_{dc} = average current over a large time interval

T_1 = time interval over which current is integrated.

Figure 7 illustrates the fluctuations in the current. To obtain the average current distribution for a number of electrons in a certain time we apply the Fourier analyses. The outcome is

$$\overline{i_b^2} = 2\, q\, I_{dc}\, \Delta f \qquad (1)$$

where

q = electron charge

Δf = frequency bandwidth of the circuit of which noise is generated.

Note that widening the bandwidth in a circuit application increases the amount of current noise.

Voltage noise. Voltage noise is due to thermal interaction between free electrons and vibration of ions in a conducting medium, which is normally a resistor. The formula[1] that expresses voltage noise in a resistor is

[1] H. Nyquist, Phys. Rev. 32. 110, 1928

$$\overline{V_R^{\ 2}} = 4\ kT\ R\ \Delta f \tag{2}$$

where

V_R = voltage across resistor

k = Boltzmann constant (1.38×10^{-23})

T = temperature Kelvin

R = resistor value

Δf = bandwidth

Note that widening the bandwidth increases the voltage noise. Thus the frequency response of the circuit determines what the noise performance will be both for voltage as well as current noise.

Since the solid state detector deposits a certain amount of charge when penetrated by an electron, we are interested in the charge due to noise. Integration of equation (1) and noting that $Q = CV$ in equation (2) to obtain charge gives us

$$\overline{Q^2_{total}} = 2\ q\ I_{dc}\ \tau + 4\ kT\ R_n\ \frac{C^2}{\tau} \tag{3}$$

where

Q = total RMS noise charge

$\tau = \frac{1}{\Delta f}$ = RC = time constant of preamplifier

R_n = main series resistor value that contributes to noise. In our case R_n is $.65 \times \frac{1}{g_m}$ for field effect transistor, g_m is transconductions.

C = total capacitance parallel to the main resistor, contributing to noise. That is, detector capacitance + field effect input cap. + wiring capacitance.

To simplify the noise calculation of the solid state detector and its preamplifier we can assume that

1. The solid state detector contributes mainly to current noise due to leakage current. The voltage noise can be neglected since R_n in equation (3) is extremely small for the detector.
2. The preamplifier noise will be mainly generated by voltage noise. As noted earlier this voltage noise depends on the value of the solid state detector capacitance. The value for R_n in the formula will be obtained from the transconductance of the FET. The current noise can be neglected since the leakage current (gate to source) for the FET will be very small compared to the leakage current of the detector. That is a factor 10-100 smaller depending on the type and selection of FET. Figures 8, 9 and 10 have been extracted from equation (3), corrected for shaping time constant. The correction factor is explained in the section on the Electronic Circuit.
3. Noise produced by parallel resistance on the detector such as bias and feedback resistors is calculated from equation (2) with Norton's theorem, that is, after integration

$$Q^2 = 4\ kT\ \frac{\tau}{R_b}$$

The effect of this source on the total noise is small, as shown in Figures 8, 9 and 10.

Temperature Dependence of Solid State Detectors. The detector is essentially a PN junction reversed biased under operating conditions. The leakage current, the main source of noise, depends on temperature. The total leakage current is given in the diode formula for small voltage potential across the diode

$$I = I_o\ (e^{qV/kT} - 1)$$

I_o is the reverse current and is mainly determined by recombination of minority carriers. For large negative voltages I_o will not be affected by voltage change since the junction contact potential is determined by the minority carrier concentration. The leakage current for large negative voltages is

$$I_o = q\, P_{no} \left(\frac{D}{\tau}\right)^{\frac{1}{2}} \tag{4}$$

D is the minority carrier diffusion coefficient, P_{no} is minority carrier concentration, q is electron charge, τ is the average life-time of minority carrier.

The minority carrier concentration is given by

$$P_{no} = P_{po}\; e^{-q\psi/kT} \tag{5}$$

P_{no} is minority carrier concentration, P_{po} is majority carrier concentration, q is electron charge, ψ is contact potential, k is Boltzmann's constant and T is temperature ^{o}K. It can be seen that the leakage current or detector noise current is highly temperature dependent. The voltage noise, however, is determined by the capacitance of the detector and input of the electronic amplifier. Cooling of the detector to obtain low current noise will not be effective, when voltage noise set by capacitance turns out to be the major cause of noise. For the detectors we are using, the operating temperature should be around -50^{o}C for sufficient performance. The performance of the system will be given later for a temperature of -50^{o}C.

<u>The Electronic Circuit.</u> The maximum counting rate that can be measured is mainly determined by the electronic circuitry. That is, the time per pulse set by RC = τ determines the noise performance. It can be seen from equation (3) that current noise is proportional to τ and voltage inversely proportional to τ. The value of τ should be determined for the type of detector to optimize noise performance. In order to keep the pulse duration short, a single differentiating-double integrating network has been designed to obtain a low noise, fast response amplifier system.

The preamplifier amplifies charge. The amplification factor is set by the feedback capacitor value. The value of RC of the feedback network determines the fall time of the voltage output pulse. This RC value is taken to be greater than 200 μ sec. The differentiating network cuts down pulse duration and low frequency noise. The integrating network cuts down high frequency noise as shown in Figure 11.

In order to obtain the best signal to noise ratio, the two noise contributions, current and voltage, should be equal. The pulse shape for optimum signal to noise ratio is approached by the single differentiation-double integration network or so called semi-Gaussian pulse shape. The equation for the voltage of the output pulse is given

$$V_{out} = \frac{2q}{C_F} e^{-t/\tau} (1 - \cos t/\tau)$$

where t is time and C_F is feedback capacitance. For RC = τ we note that the pulse oscillates (under damped) as shown in Figure 12.

The second pulse height can be neglected since this is only $e^{-2\pi} = 1/530$ of the height of the first pulse.

From Figure 12 can be seen that maximum count rate can be as high as 200 kc/sec without substantial pulse height distortion. For randomly counted pulses one usually takes 1/10 of this number, 20 k pulses/sec.

The noise equation (3) has been corrected for single differentiation and single and double integration network and is

	Voltage Noise	Current Noise
Double integration	(6) $2.3\ kT\ R\ \frac{C^2}{\tau}$	(7) $1.73\ q\ I_{dc}\ \tau$
Single integration	(8) $3.7\ kT\ R\ \frac{C^2}{\tau}$	(9) $1.85\ q\ I_{dc}\ \tau$

Equations (6) and (7) were used to calculate the noise and fwhm resolution for surface barrier detectors and their electronics. The results are tabulated in Table 9. The leakage current of the detector for various temperatures is an average value of several detectors to be used on the IMP spacecraft. Similar detectors will be flown on the Apollo subsatellite. Figure 13 is a plot of the leakage current versus temperature.

Two versions of preamplifiers have been developed for low capacitance detectors and high capacitance detectors. The low capacitance version, shown in Figure 14 and used to measure lithium drifted detectors, differs from the regular preamplifiers in the following ways

1. The field effect transistor has to be selected for low leakage gate current.
2. The field effect transistor is mounted next to the detector to eliminate wire capacitance.
3. The feedback and bias resistors are mounted next to the detector and should be cooled to detector operating temperature to diminish current noise of the preamplifier.
4. The second stage of the preamplifier has been designed with field effect transistors to eliminate additional transistor shot noise.

The high capacitance version is shown in Figure 15 together with the main amplifiers and shaping networks. The performance of the preamplifiers are shown in Figures 16 and 17.

Experimental Data. Measurements have been done on noise performance on two types of detectors, lithium drifted and surface barrier detectors. Figure 18 shows a block diagram of the set up. The detectors were cooled in vacuum so that no impurities such as moisture and organic vapors could deteoriate the detector during test. Noise figures obtained are shown in Table 10. Figure 19 shows pulse height spectra obtained from the Kevex 1193 detector.

Detector Lifetime

A series of long-term tests were run on surface barrier detectors similar to those being flown on the subsatellite. These tests were primarily to evaluate the effects of radiation on the detectors in a flight environment. In particular, efforts were concentrated on measuring the degradation in noise performance. Measurements indicate that such effects are the first signs of radiation damage, but they do not provide a quantitative measure of the extent of such degradation with accumulated particle flux. Our tests are designed to provide such quantitative measurements.

In the tests a telescope made up of three surface barrier detectors, two 25 mm^2 area-300 μ thick and one 50 mm^2-300 μ, was placed in a vacuum of ≤ 5 microns and at a temperature of -30°C. Electrons of energies up to 2.2 MeV from a Sr^{90} source are used to irradiate the detectors. These electrons penetrate all three detectors. Count rates of $\sim 10^4$ counts/second were maintained for 125 hours to provide a total of $\sim 5 \times 10^9$ counts. The noise in the detectors was monitored in three ways (1) by an rms noise meter, (2) by counting rate above initial threshold (set at 1 count/minute), (3) by observing pulser counting rate into a single channel analyzer containing most of the pulser peak. This is a measure of the change in the fwhm of the peak. These tests are continuing at the present time, although the accumulated counts are already beyond that expected for a full year's operation in lunar orbit. The results are essentially negative noise measured by the rms meter has changed by $\leq 2\%$, just barely above the accuracy of the measurement. The other two measurements are less sensitive and show no noticeable change.

Table 1. ANALYZER CHARACTERISTICS

Detector	Inside Radius R_1 (cm)	Outside Radius R_2 (cm)	Applied Voltage V (volts)	Energy Range: ½ Max Low E_{min} (keV)	Energy Range: ½ Max High E_{max} (keV)	Peak Geometric Factor g ($cm^2 \cdot sr$)	Total Geometric Factor G ($cm^2 \cdot sr \cdot keV$)
C_1	2.25	2.74	300	0.58	0.65	3.2×10^{-3}	1.4×10^{-4}
C_2	2.25	2.75	1000	1.93	2.17	3.2×10^{-3}	4.7×10^{-4}
C_3	4.5	5.5	3000	5.73	6.40	3.3×10^{3}	1.4×10^{-3}
C_4	4.5	5.5	3000	5.65	6.55	0.48	0 27
C_5	4.625	5.375	5000	13.6	15.0	0.70	0.63

Table 2. TRANSMISSION MATRIX FOR C_1 (CM^2)

Energy (keV)	INCIDENT ANGLE (DEGREES)							
	-6	-4	-2	0	2	4	6	8
0.58	0.0016	0.0044	0.0059	0.0064	0.0040	0	0	0
0.59	0.0076	0.0101	0.0101	0.0101	0.0101	0.0011	0	0
0.60	0.0092	0.0101	0.0101	0.0101	0.0101	0.0099	0	0
0.61	0	0.0101	0.0101	0.0101	0.0101	0.0101	0	0
0.62	0	0.0101	0.0101	0.0101	0.0101	0.0101	0.0101	0
0.63	0	0	0.0101	0.0101	0.0101	0.0101	0.0101	0
0.64	0	0	0.0101	0.0101	0.0101	0.0101	0 0101	0
0.65	0	0	0.0017	0.0066	0.0074	0.0095	0.0101	0.0089
0.66	0	0	0	0	0.0002	0.0024	0.0060	0.0101
0.67	0	0	0	0	0	0	0	0.0037

Table 3. TRANSMISSION MATRIX FOR C_2 (CM^2)

Energy (keV)	INCIDENT ANGLE (DEGREES) -6	-4	-2	0	2	4	6	8
1.93	0.0016	0.0044	0.0059	0.0064	0.0040	0	0	0
1.97	0.0076	0.0101	0.0101	0.0101	0.0101	0.0011	0	0
2.00	0.0092	0.0101	0.0101	0.0101	0.0101	0.0099	0	0
2.04	0	0.0101	0.0101	0.0101	0.0101	0.0101	0	0
2.07	0	0.0101	0.0101	0.0101	0.0101	0 0101	0.0101	0
2.10	0	0	0.0101	0.0101	0.0101	0.0101	0.0101	0
2.14	0	0	0.0101	0.0101	0.0101	0.0101	0.0101	0
2.17	0	0	0.0017	0.0066	0.0074	0.0095	0.0101	0.0089
2.20	0	0	0	0	0.0002	0.0024	0.0060	0.0101
2.24	0	0	0	0	0	0	0	0.0037

Table 4. TRANSMISSION MATRIX FOR C_3 (CM^2)

Energy (keV)	INCIDENT FLUX (DEGREES) -6	-4	-2	0	2	4	6	8
5.72	0.0004	0.0057	0.0089	0.0099	0.0044	0	0	0
5.80	0.0097	0.0101	0.0101	0.0101	0.0101	0	0	0
5.87	0.0101	0.0101	0.0101	0.0101	0.0101	0.0062	0	0
5.95	0.0101	0.0101	0.0101	0.0101	0.0101	0.0101	0	0
6.02	0.0101	0.0101	0.0101	0.0101	0.0101	0.0101	0	0
6.10	0	0.0101	0.0101	0.0101	0.0101	0.0101	0	0
6.17	0	0.0101	0.0101	0.0101	0.0101	0.0101	0.0101	0
6.25	0	0.0060	0.0101	0.0101	0.0101	0.0101	0.0101	0
6.32	0	0	0.0101	0.0101	0.0101	0.0101	0.0101	0
6.40	0	0	0.0024	0.0094	0.0101	0.0101	0.0101	0
6.47	0	0	0	0	0	0.0039	0.0101	0.045
6.55	0	0	0	0	0	0	0	0.0101

Table 5. TRANSMISSION MATRIX FOR C_4 (CM^2)

Energy (keV)	INCIDENT ANGLE (DEGREES) -6	-4	-2	0	2	4	6	8
5.35	0.02	0.15	0.20	0.22	0	0	0	0
5.50	0.37	0.50	0.50	0.57	0	0	0	0
5.65	0.72	0.85	0.90	0.92	0.65	0	0	0
5.80	1.10	1.22	1.27	1.30	1.10	0	0	0
5.95	1.10	1.60	1.65	1.67	1.52	0.95	0	0
6.10	0	1.35	1.80	1.95	1.95	1.52	0	0
6.25	0	0.50	1.35	1.52	1.55	1.65	1.25	0
6.40	0	0	0.80	1.10	1.12	1.20	1.35	0.20
6.55	0	0	0	0.65	0.67	0.75	0.90	1.12
6.70	0	0	0	0.17	0 20	0 27	0.42	0.63
6.85	0	0	0	0	0	0	0	0.12

Table 6. TRANSMISSION MATRIX FOR C_5 (CM^2)

Energy (keV)	INCIDENT ANGLE (DEGREES) -6	-4	-2	0	2	4	6	8
13.10	0	0.28	0.47	0.52	0	0	0	0
13 25	0.37	0.66	0.84	0.89	0	0	0	0
13.40	0.80	1.08	1.27	1.31	0	0	0	0
13.55	1.22	1.50	1.64	1.73	0.28	0	0	0
13.70	1.50	1.92	2.06	2.16	1.31	0	0	0
13.85	0	2.34	2.53	2.58	1.92	0	0	0
14.00	0	2.72	2.95	3.00	2.44	0	0	0
14 15	0	2.16	3 37	3.42	2.91	0	0	0
14.30	0	0.98	3.19	3.66	3 47	1.69	0	0
14.45	0	0	2.62	3.19	3.28	2 53	0	0
14.60	0	0	2.02	2.72	2 81	3 00	0	0
14.75	0	0	1.31	2.22	2.30	2 53	1 08	0
14.90	0	0	0	1 78	1.83	2 06	2 02	0
15.05	0	0	0	1 27	1 36	1.55	1.64	0
15.20	0	0	0	0.75	0.84	1.03	1 13	0
15.35	0	0	0	0.23	0.33	0.52	0 61	0
15.50	0	0	0	0	0	0	0 05	0 84

Table 7 BACKGROUND LEVEL REQUIREMENTS

Analyzer	Minimum Detectable Flux	Count Rate	Maximum Background Level	Design Goal
C_1	10^4	1.4	0.6	0.1
C_2	10^4	4.7	3.0	0.1
C_3	10^3	1.4	0.6	0.1
C_4	1	0.27	0.1	0.1
C_5	1	0.63	0.2/4* = 0 05	0.01

*Divide by 4 since the C_5 detector is sectored and all solar UV counts may fall into one sector.

Table 8. PREDICTION OF BACKGROUND COUNT RATE DUE TO SOLAR UV (COUNTS/SEC)

Analyzer	No Sunshade No Serration	No Sunshade 11° Serrations	2" Sunshade 11° Serrations	2" Sunshade 35° Serrations	Design Goal
C_1	6.1^{+}	2.2^{+}	0.65^{+}	0.12^{*}	0.1
C_2	6.1^{+}	2.2^{+}	0.65^{+}	0.12^{*}	0.1
C_3	0.4^{+}	0.2^{+}	0.1^{+}	0.0032^{*}	0.1
C_4	43^{*}	16^{*}	1.3^{*}	0.32^{*}	0.1
C_5	1.1^{*}	0.38^{*}	0.078^{*}	0.0079^{*}	$0.01^{\dagger}$

*Experimentally verified.

$^{+}$Prediction based on experimental results.

$^{\dagger}C_5$ detector has stricter requirements since all solar UV counts may fall into one sector.

Table 9. SYSTEM NOISE VS. TEMPERATURE

Detector Temperature	I Leakage	τ μ sec	.25 μ sec	1 μ sec	4 μ sec
		Q^2 detector	$.34 \times 10^{-32}$	1.35×10^{-32}	5.1×10^{-32}
+20°C	50 nA	Q^2 preamp	92×10^{-34}	23×10^{-34}	6×10^{-34}
		fwhm	6 keV	6.7 keV	11 keV
		Q^2 detector	4.7×10^{-34}	19×10^{-34}	75×10^{-34}
0°C	7 nA	Q^2 preamp	92×10^{-34}	23×10^{-34}	6×10^{-34}
		fwhm	5.2 keV	3.2 keV	4.5 keV
		Q^2 detector	1.35×10^{-34}	5.4×10^{-34}	21.5×10^{-34}
-20°C	2 nA	Q^2 preamp	92×10^{-34}	23×10^{-34}	6×10^{-34}
		fwhm	5.15 keV	2.85 keV	2.75 keV
		Q^2 detector	$.65 \times 10^{-34}$	2.7×10^{-34}	11×10^{-34}
-40°C	1 nA	Q^2 preamp	92×10^{-34}	23×10^{-34}	6×10^{-34}
		fwhm	5.15 keV	2.7 keV	2.2 keV

Detector capacitance is 50 pf, preamp resistance is $R = 0.65(1/g_m) = 100\,\Omega$.

Preamplifier temperature is kept at 290 °K.

fwhm is 2.35 × RMS noise, 1.6×10^{-19} coulombs, corresponds to 3.6 eV deposited in the detector.

Table 10. NOISE MEASUREMENTS ON DETECTORS

	Lithium Drift Detector (Kevex 1178)	Lithium Drift Detector (Kevex 1193)	Surface Barrier Detector (Nuclear Diodes)
Total Capacitance Detector and input preamplifier	10 pf	12 pf	70 pf
Leakage at -50°C for Lithium	<1 nA	<1 nA	Leakage at -30°C <5 nA
Noise (fwhm)	1 keV	1.2 keV	5 keV
Noise Threshold Level for 1 count/minute	2.7 keV	3 keV	12 keV

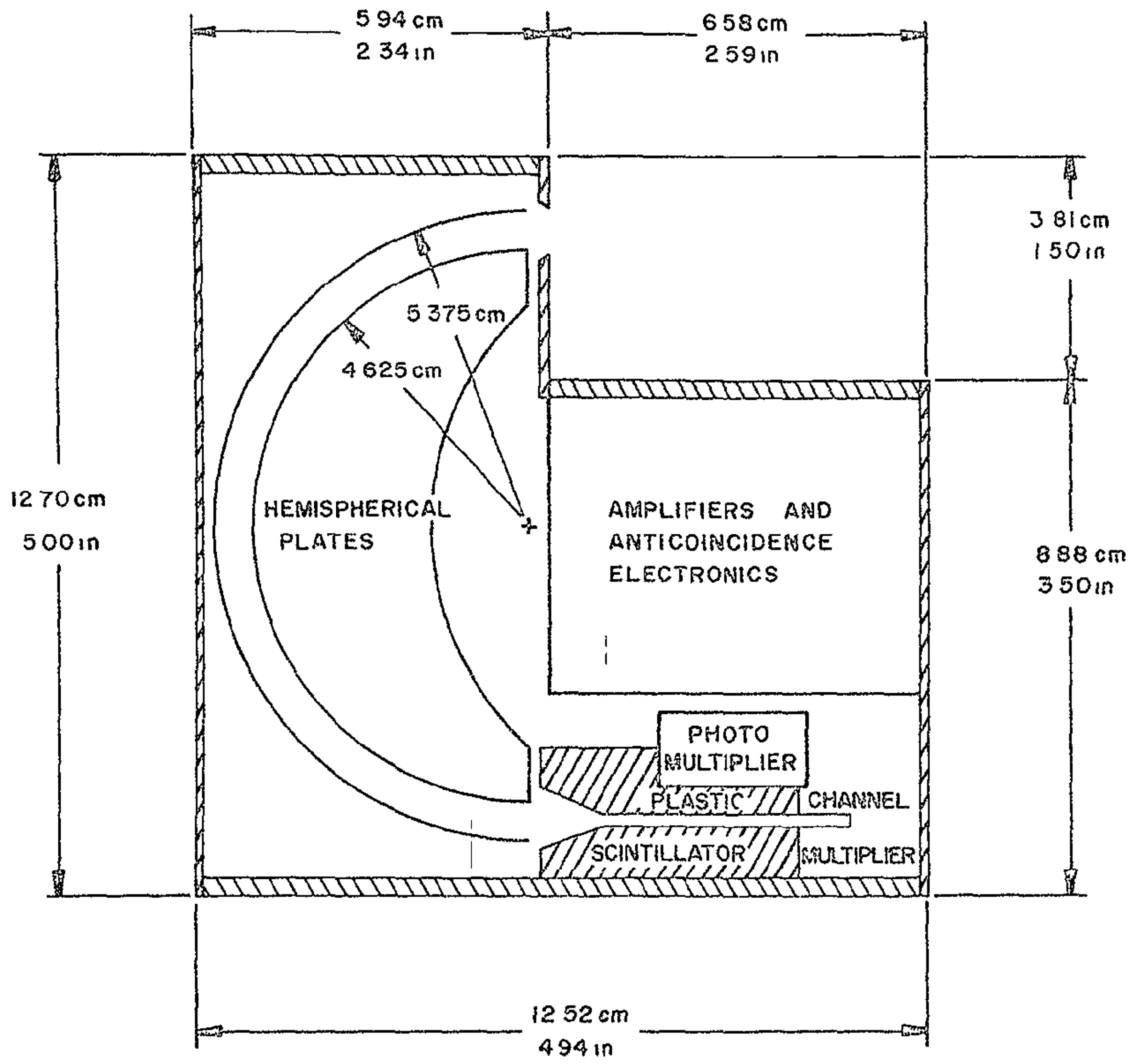
5 94 cm
2 34 in
6 58 cm
2 59 in
3 81 cm
1 50 in
5 375 cm
4 625 cm
12 70 cm
5 00 in
HEMISPHERICAL
PLATES
AMPLIFIERS AND
ANTICOINCIDENCE
ELECTRONICS
8 88 cm
3 50 in
PHOTO
MULTIPLIER
PLASTIC
SCINTILLATOR
CHANNEL
MULTIPLIER
12 52 cm
4 94 in

Figure 1

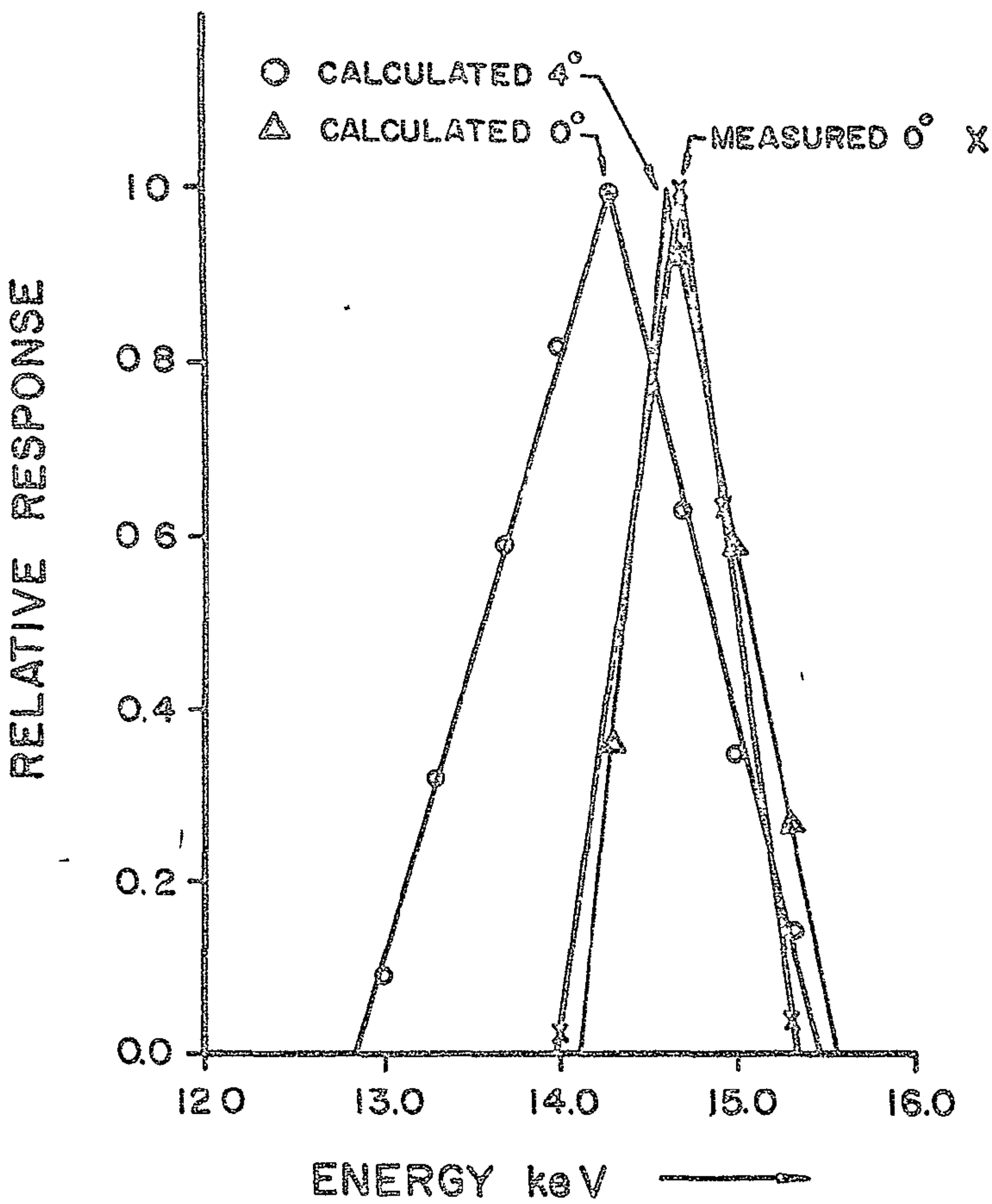

O CALCULATED 4°
△ CALCULATED 0°
MEASURED 0° X
RELATIVE RESPONSE
1.0
0.8
0.6
0.4
0.2
0.0
12.0
13.0
14.0
15.0
16.0
ENERGY keV

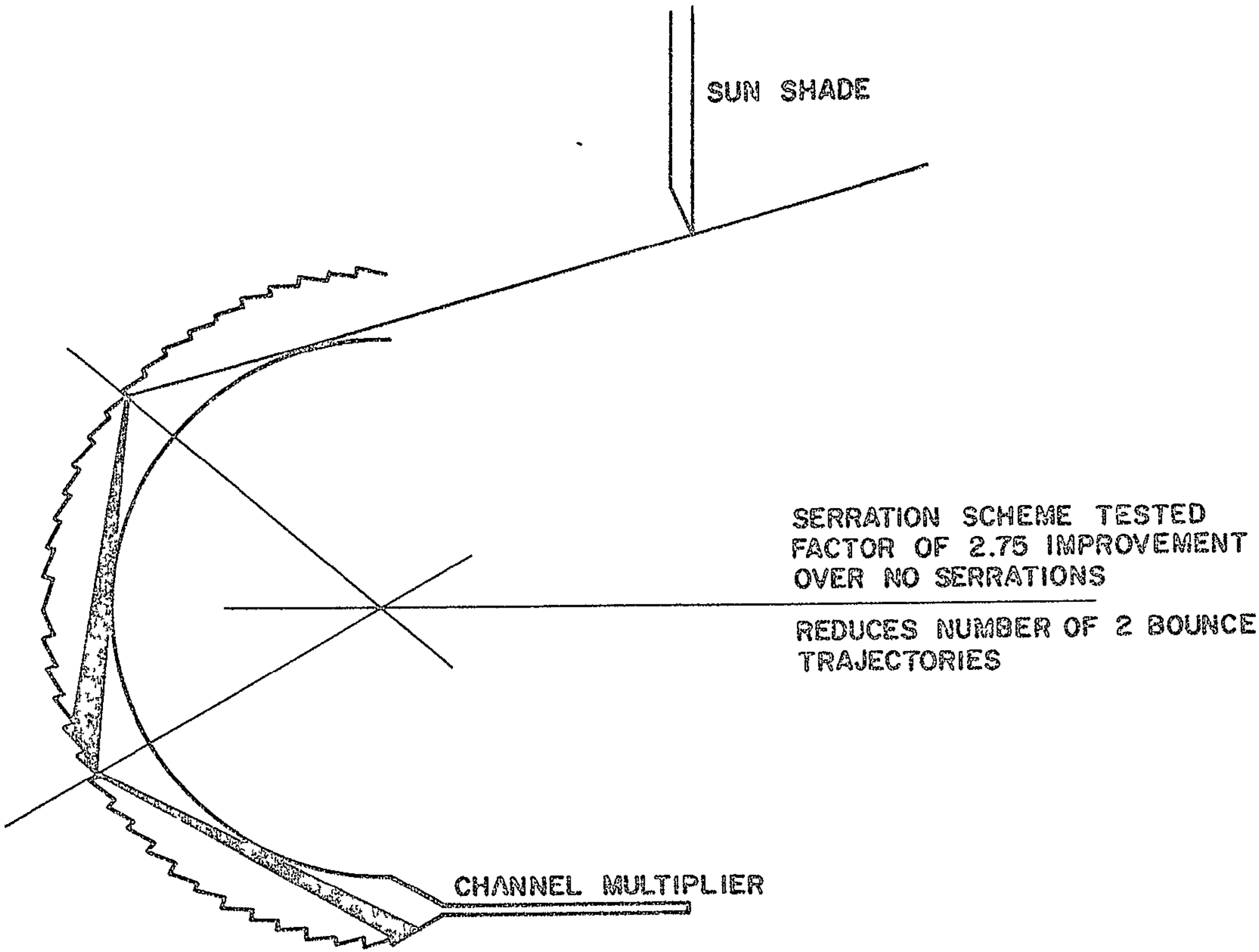
SUN SHADE
SERRATION SCHEME TESTED
FACTOR OF 2.75 IMPROVEMENT
OVER NO SERRATIONS
REDUCES NUMBER OF 2 BOUNCE
TRAJECTORIES
CHANNEL MULTIPLIER

Figure 3

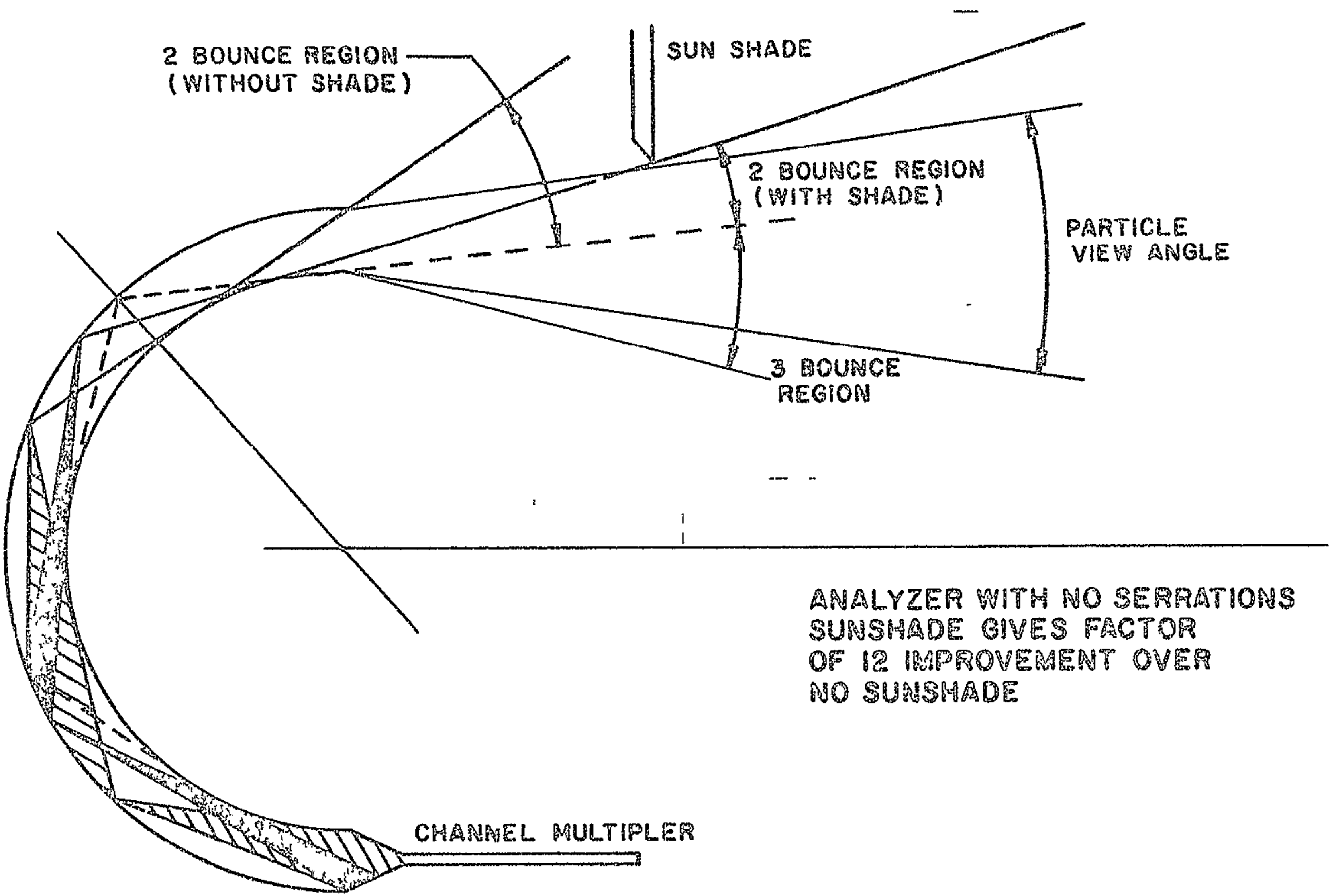
2 BOUNCE REGION
(WITHOUT SHADE)
SUN SHADE
2 BOUNCE REGION
(WITH SHADE)
PARTICLE
VIEW ANGLE
3 BOUNCE
REGION
ANALYZER WITH NO SERRATIONS
SUNSHADE GIVES FACTOR
OF 12 IMPROVEMENT OVER
NO SUNSHADE
CHANNEL MULTIPLER

Figure 4

COSMIC RAY ANTI COINCIDENCE TEST

LAB MODEL OF C_5 ANALYZER

TEST SET UP

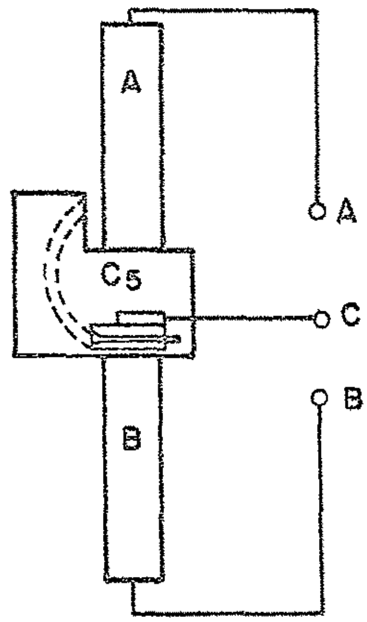

COINCIDENCE	NO.	TIME	RATE
A + B	499	2309 MIN	0 216 $\frac{\text{COUNTS}}{\text{MIN}}$
A + B + C	480	3971	0 129
A + B (ACCIDENTAL)	13	974	0 013

EFFICIECY 63 %

Figure 5

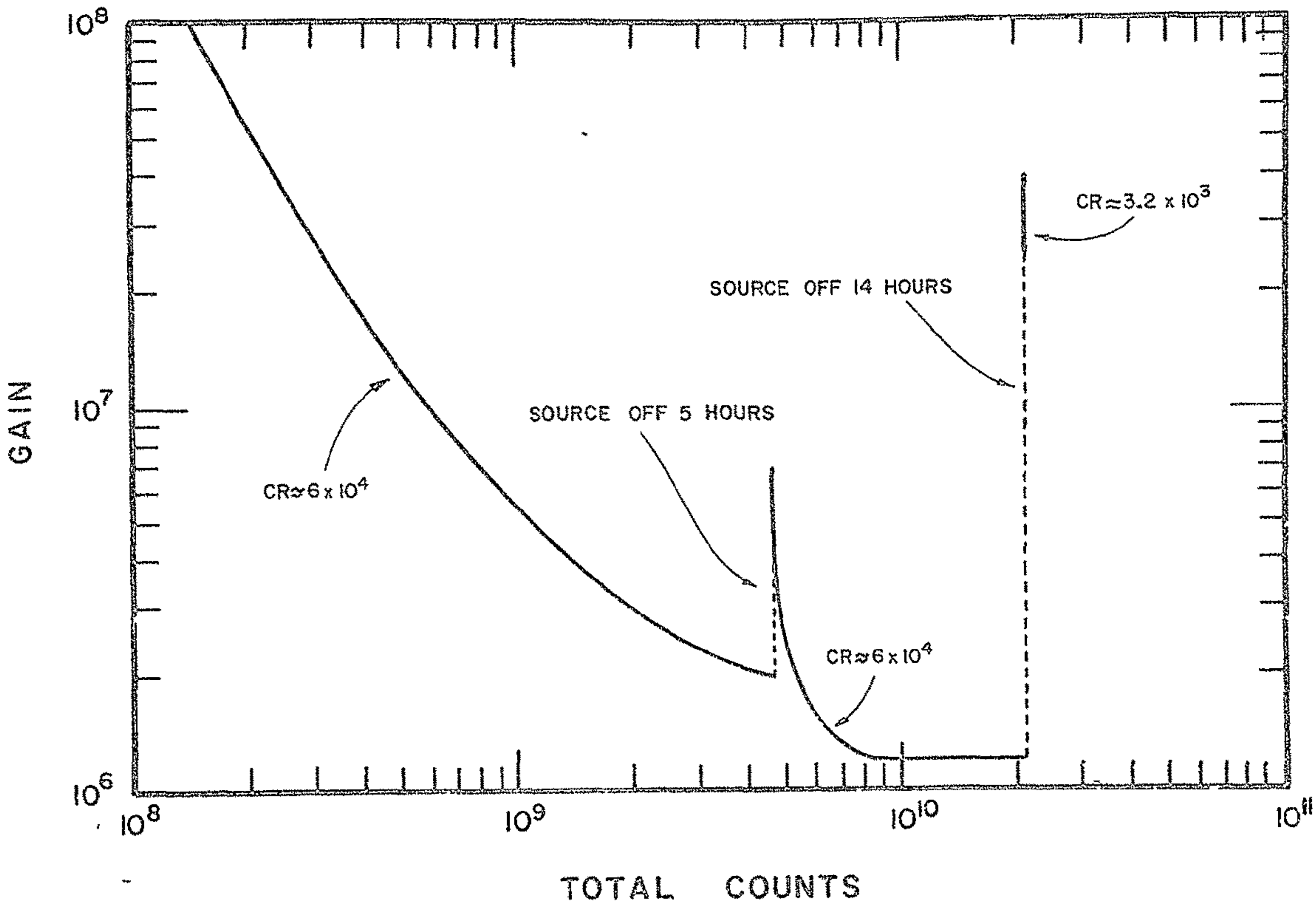

GAIN
TOTAL COUNTS
SOURCE OFF 14 HOURS
SOURCE OFF 5 HOURS
CR≈3.2 x 10³
CR≈6 x 10⁴
CR≈6 x 10⁴
10⁸
10⁷
10⁶
10⁸
10⁹
10¹⁰
10¹¹

Figure 6

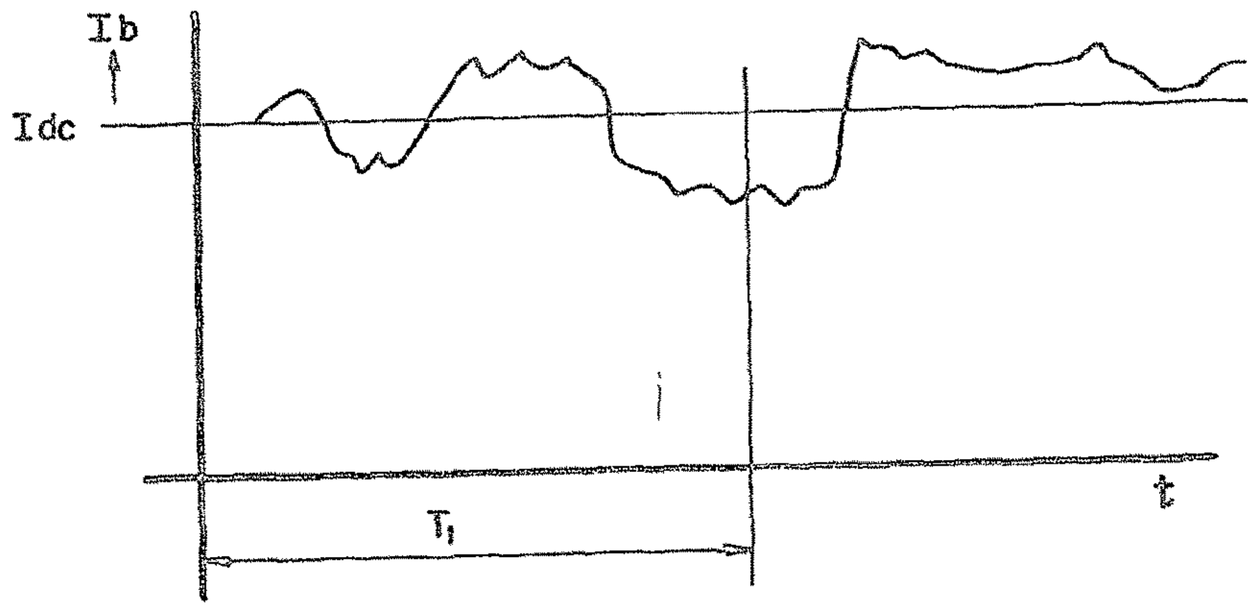

Figure 7

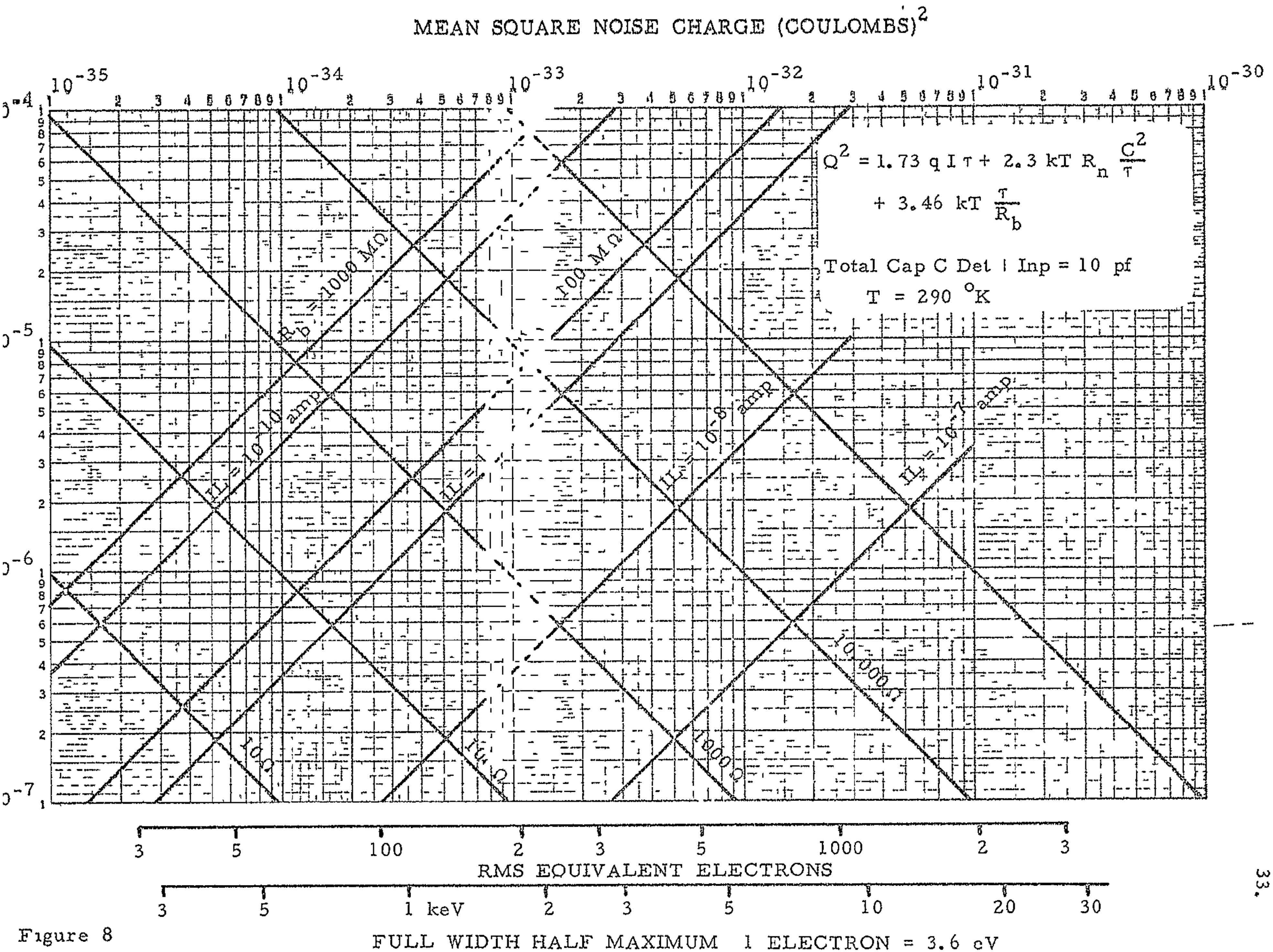
MEAN SQUARE NOISE CHARGE (COULOMBS)^2
10^{-35}
10^{-34}
10^{-33}
10^{-32}
10^{-31}
10^{-30}
$Q^2 = 1.73\, q\, I\, \tau + 2.3\, kT\, R_n \frac{C^2}{\tau} + 3.46\, kT \frac{\tau}{R_b}$
Total Cap C Det | Inp = 10 pf
T = 290 °K
R_b = 1000 MΩ
100 MΩ
$I_L = 10^{-10}$ amp
I_L =
$I_L = 10^{-8}$ amp
$I_L = 10^{-7}$ amp
10,000 Ω
1000 Ω
10 Ω
RMS EQUIVALENT ELECTRONS
3
5
100
2
3
5
1000
2
3
1 keV
10
20
30
FULL WIDTH HALF MAXIMUM 1 ELECTRON = 3.6 eV
Figure 8

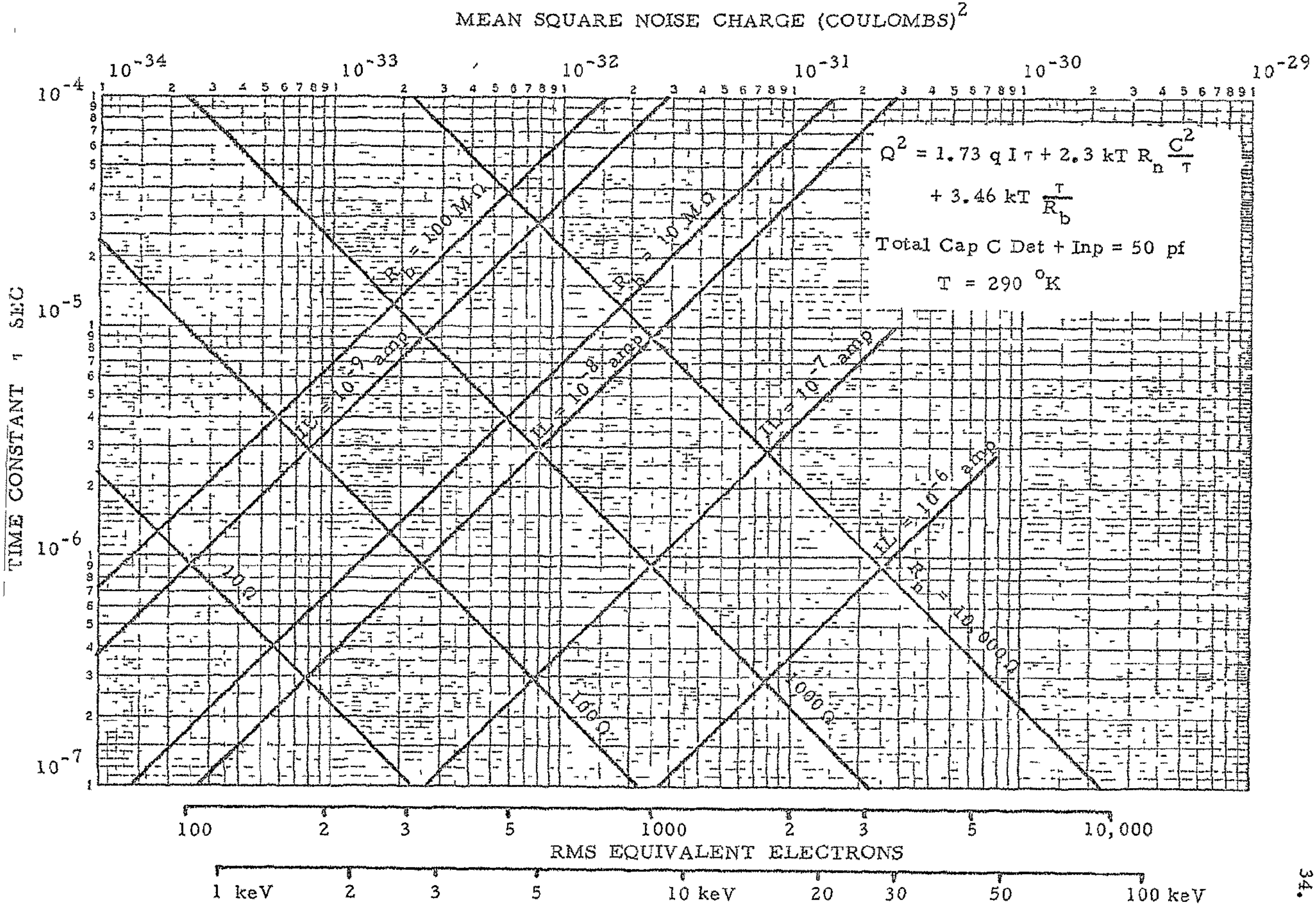

MEAN SQUARE NOISE CHARGE (COULOMBS)^2
10^{-34}
10^{-33}
10^{-32}
10^{-31}
10^{-30}
10^{-29}
TIME CONSTANT τ SEC
10^{-4}
10^{-5}
10^{-6}
10^{-7}
$Q^2 = 1.73\, q\, I\, \tau + 2.3\, kT\, R_n \frac{C^2}{\tau} + 3.46\, kT \frac{\tau}{R_b}$
Total Cap C Det + Inp = 50 pf
T = 290 ^{o}K
R_b = 100 MΩ
R_b = 10 MΩ
IL = 10^{-9} amp
IL = 10^{-8} amp
IL = 10^{-7} amp
IL = 10^{-6} amp
R_n = 10,000 Ω
1000 Ω
100 Ω
10 Ω
100
2
3
5
1000
2
3
5
10,000
RMS EQUIVALENT ELECTRONS
1 keV
2
3
5
10 keV
20
30
50
100 keV
FULL WIDTH HALF MAXIMUM 1 ELECTRON = 3.6 eV

Figure 9

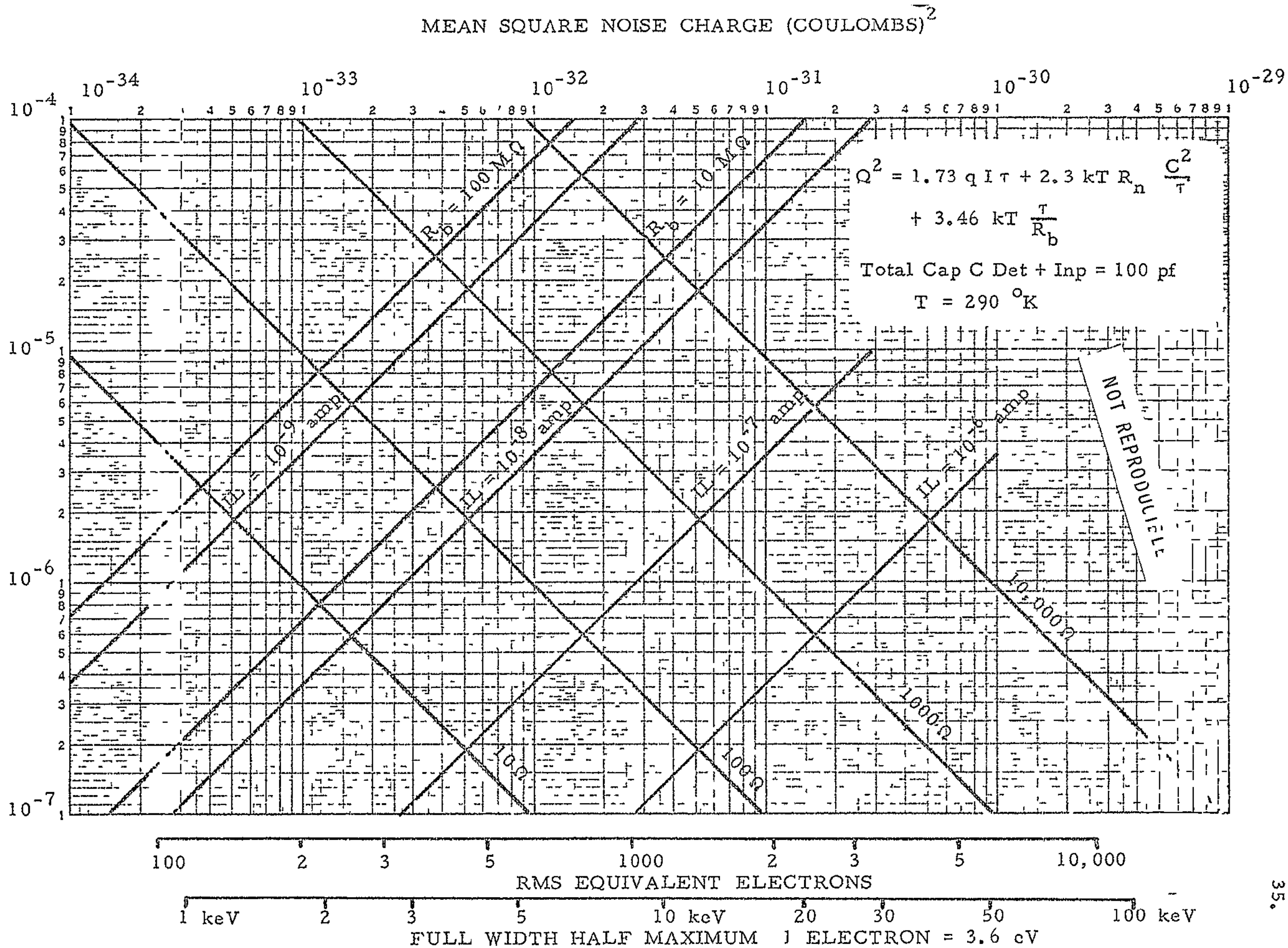
MEAN SQUARE NOISE CHARGE (COULOMBS)²
10⁻³⁴
10⁻³³
10⁻³²
10⁻³¹
10⁻³⁰
10⁻²⁹
10⁻⁴
10⁻⁵
10⁻⁶
10⁻⁷
Q² = 1.73 q I τ + 2.3 kT Rn C²/τ + 3.46 kT τ/Rb
Total Cap C Det + Inp = 100 pf
T = 290 °K
Rb = 100 MΩ
Rb = 10 MΩ
IL = 10⁻⁹ amp
IL = 10⁻⁸ amp
IL = 10⁻⁷ amp
IL = 10⁻⁶ amp
10,000 Ω
1000 Ω
100 Ω
10 Ω
NOT REPRODUCIBLE
100
2
3
5
1000
2
3
5
10,000
RMS EQUIVALENT ELECTRONS
1 keV
2
3
5
10 keV
20
30
50
100 keV
FULL WIDTH HALF MAXIMUM 1 ELECTRON = 3.6 eV

Figure 10

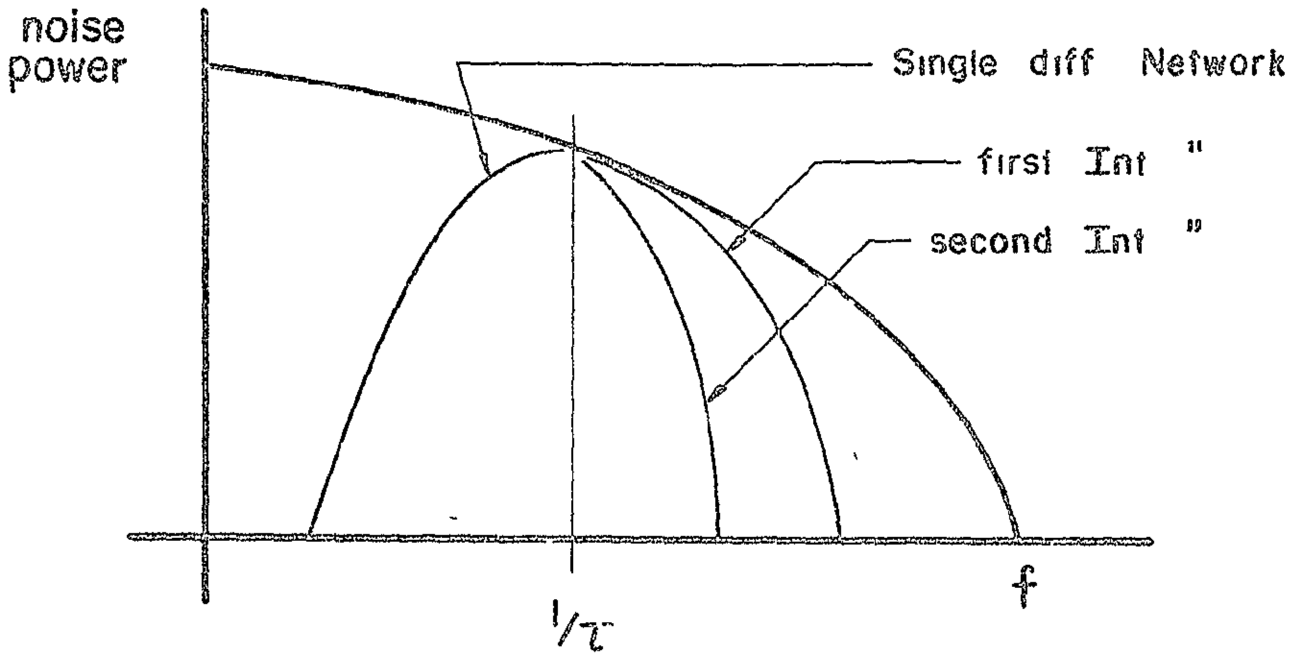

Figure 11

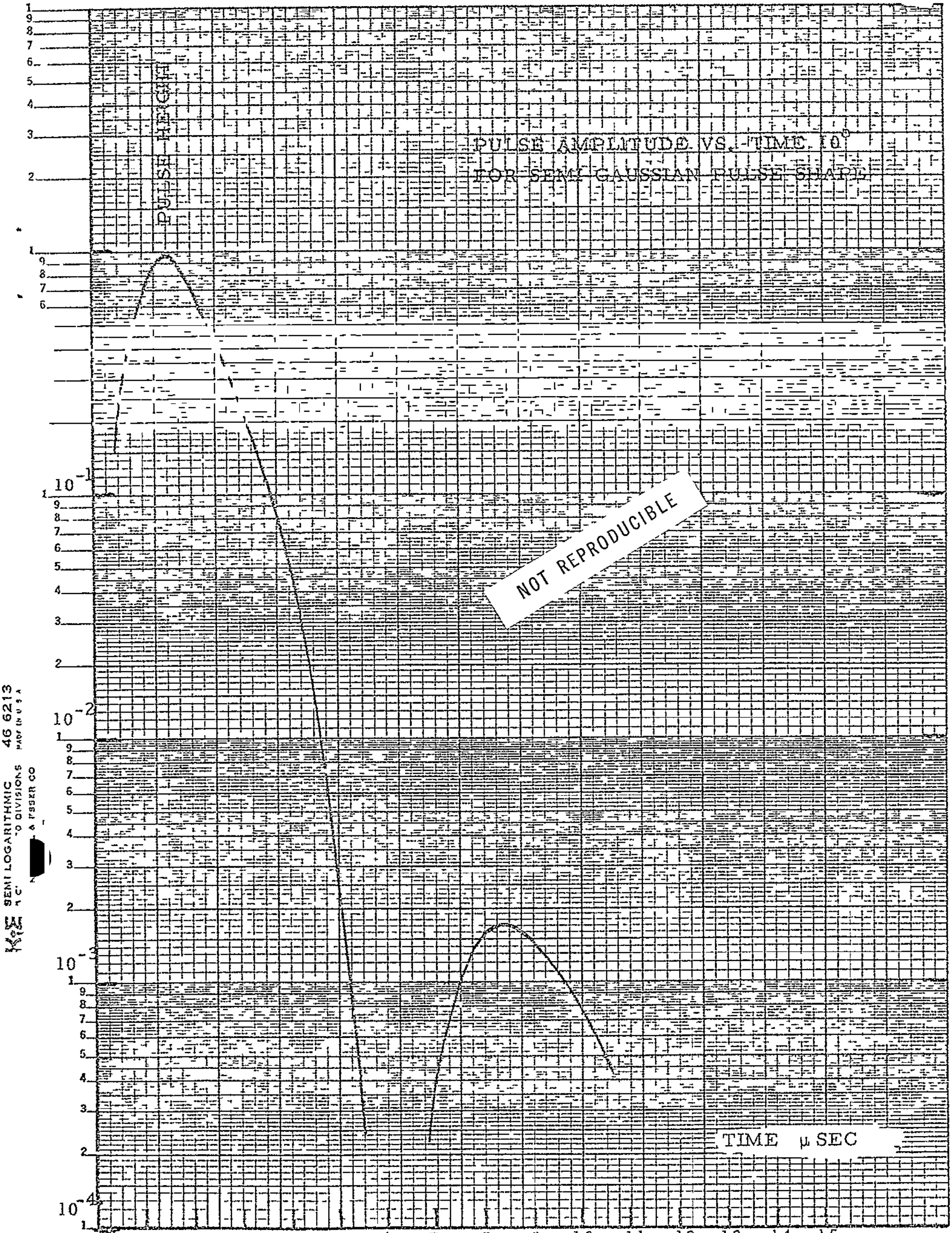
PULSE AMPLITUDE VS. TIME 10^{0}
FOR SEMI GAUSSIAN PULSE SHAPE
PULSE HEIGHT
NOT REPRODUCIBLE
10^{-1}
10^{-2}
10^{-3}
10^{-4}
TIME μ SEC
1 2 3 4 5 6 7 8 9 10 11 12 13 14 15
SEMI LOGARITHMIC
46 6213

Figure 12

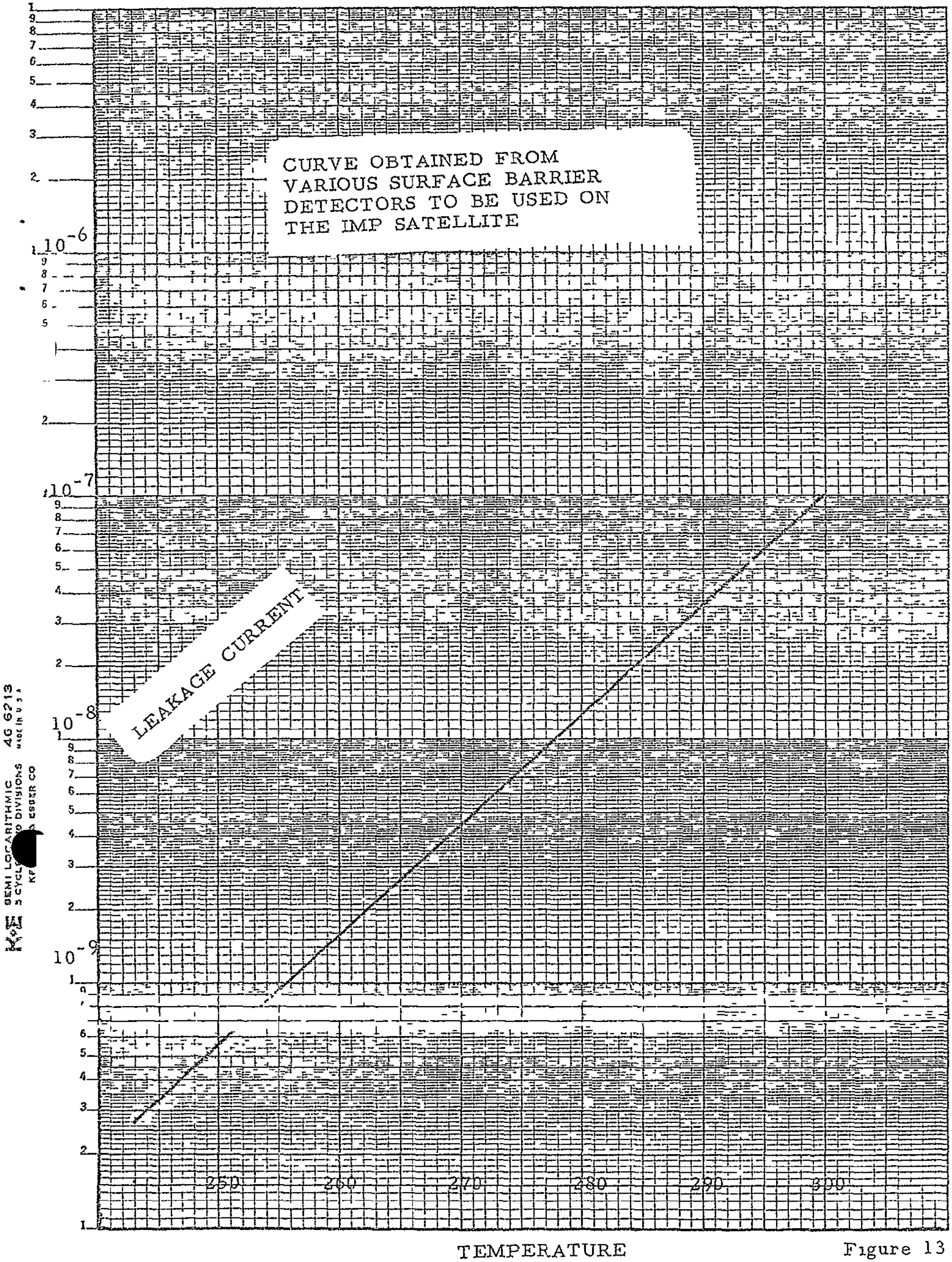
CURVE OBTAINED FROM
VARIOUS SURFACE BARRIER
DETECTORS TO BE USED ON
THE IMP SATELLITE
LEAKAGE CURRENT
10^{-6}
10^{-7}
10^{-8}
10^{-9}
250
260
270
280
290
300
TEMPERATURE
SEMI LOGARITHMIC 46 6213
5 CYCLES X 70 DIVISIONS
KEUFFEL & ESSER CO

Figure 13

Low Cap Low Noise Preampl.

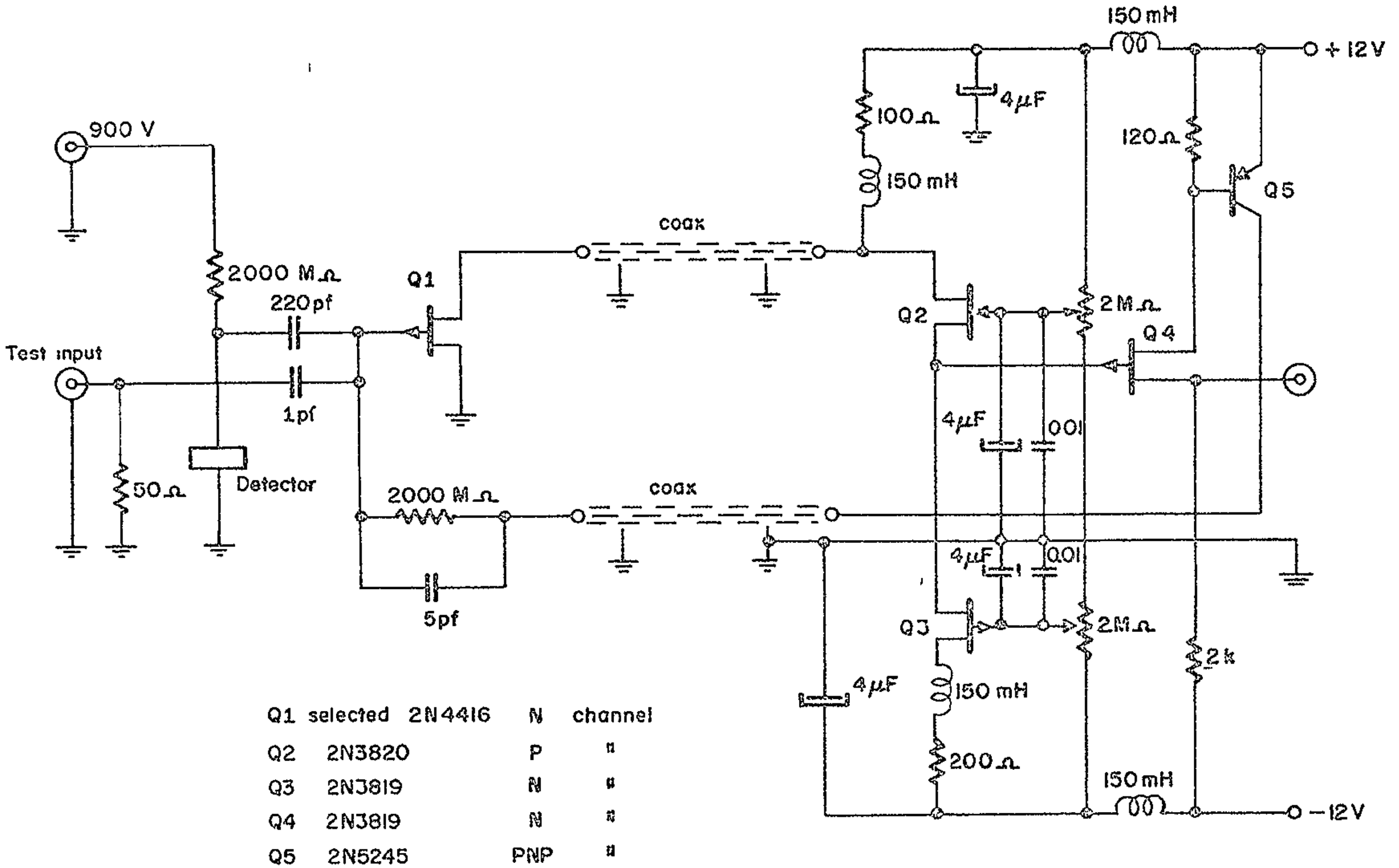

Figure 14

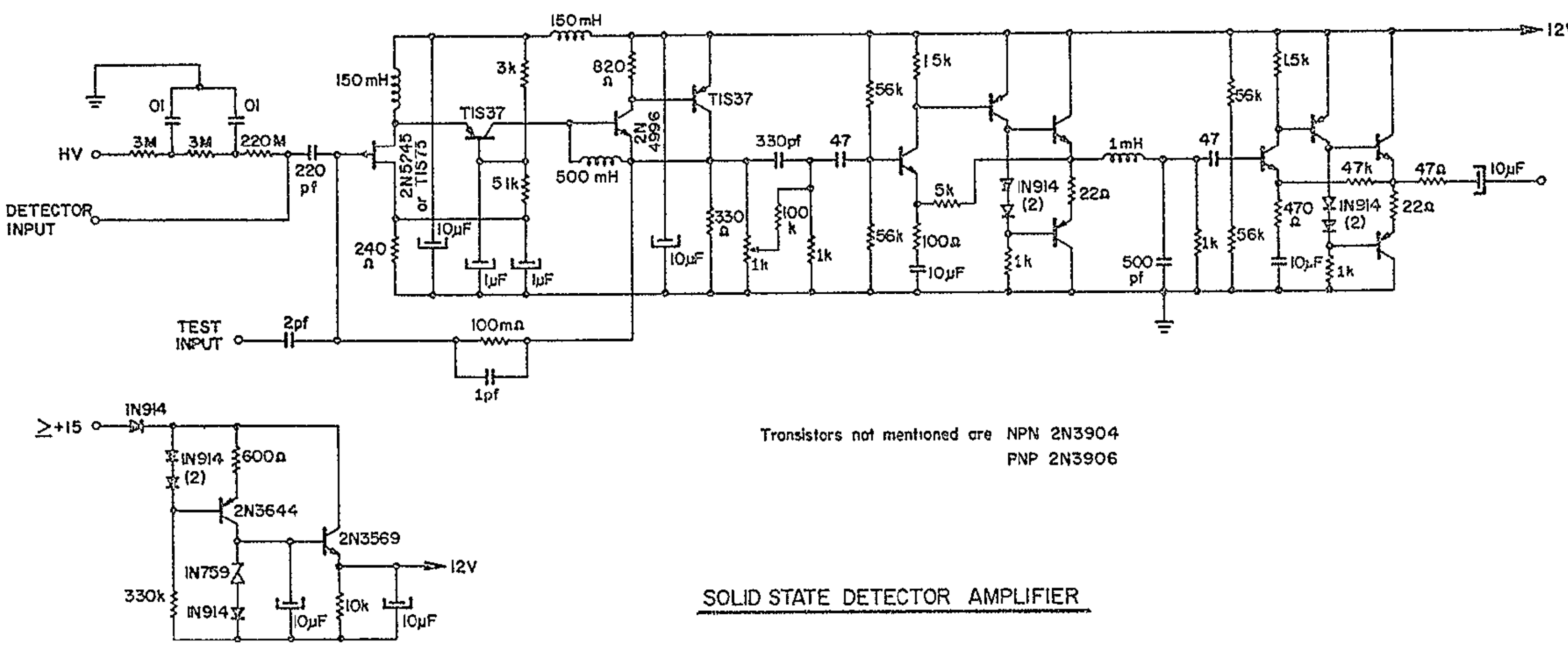

SOLID STATE DETECTOR AMPLIFIER

Figure 15

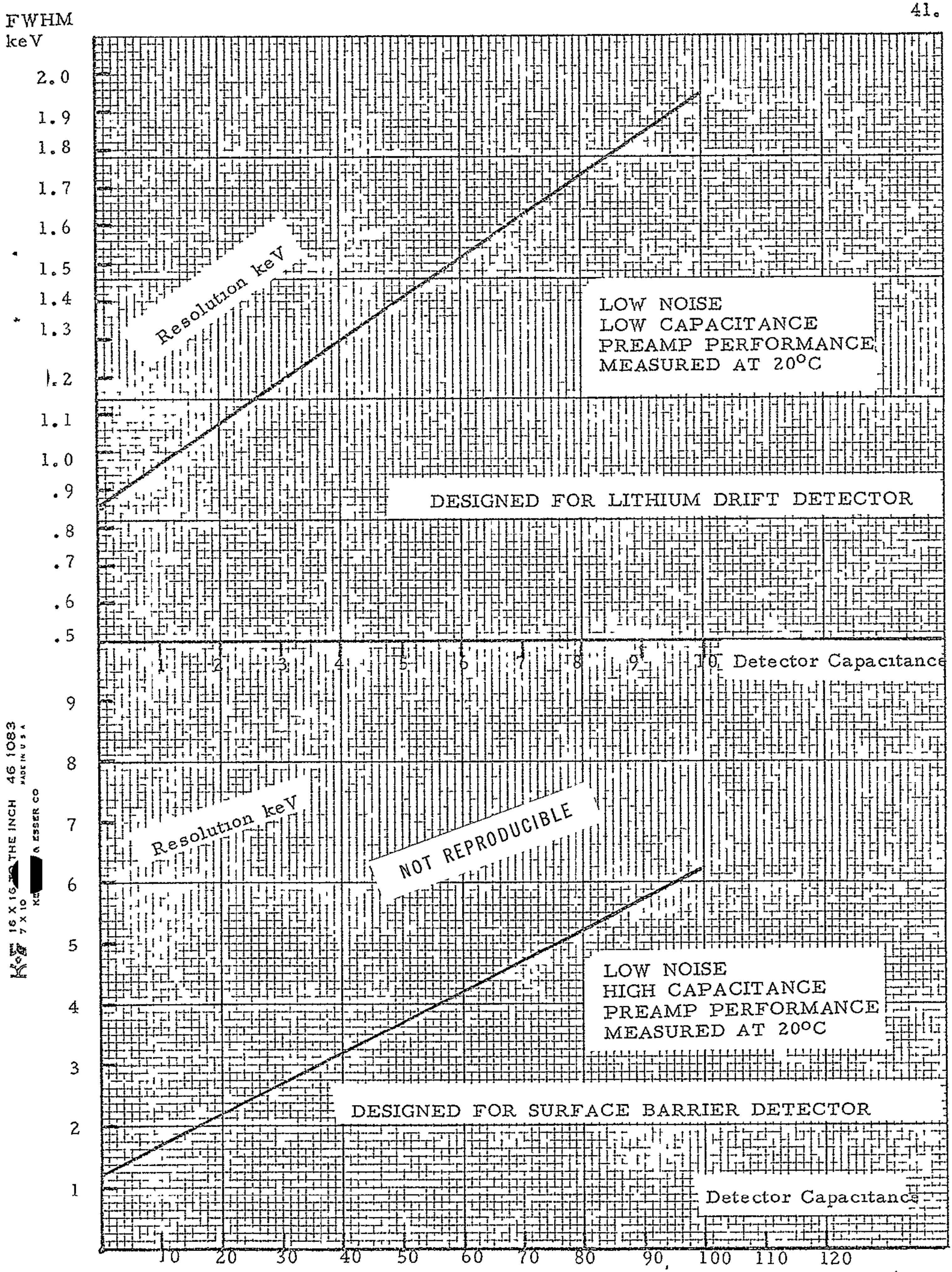
FWHM
keV
2.0
1.9
1.8
1.7
1.6
1.5
1.4
1.3
1.2
1.1
1.0
.9
.8
.7
.6
.5
Resolution keV
LOW NOISE
LOW CAPACITANCE
PREAMP PERFORMANCE
MEASURED AT 20°C
DESIGNED FOR LITHIUM DRIFT DETECTOR
1
2
3
4
5
6
7
8
9
10
Detector Capacitance
9
8
7
6
5
4
3
2
1
Resolution keV
NOT REPRODUCIBLE
LOW NOISE
HIGH CAPACITANCE
PREAMP PERFORMANCE
MEASURED AT 20°C
DESIGNED FOR SURFACE BARRIER DETECTOR
Detector Capacitance
10
20
30
40
50
60
70
80
90
100
110
120

OUTPUT VOLTAGE
Preamplifier + Main Amplifier -- High Capacitance Version

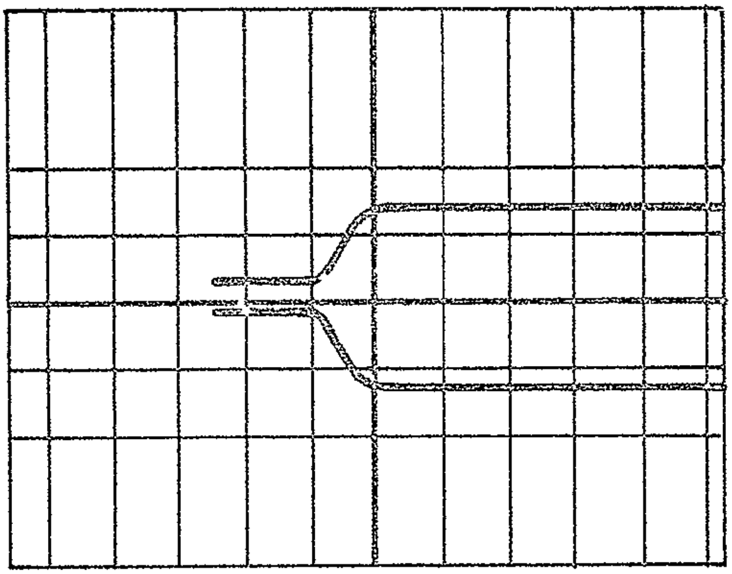

Input tail pulser

Output charge preamplifier with 0 pf input capacitance

50 n sec/div.

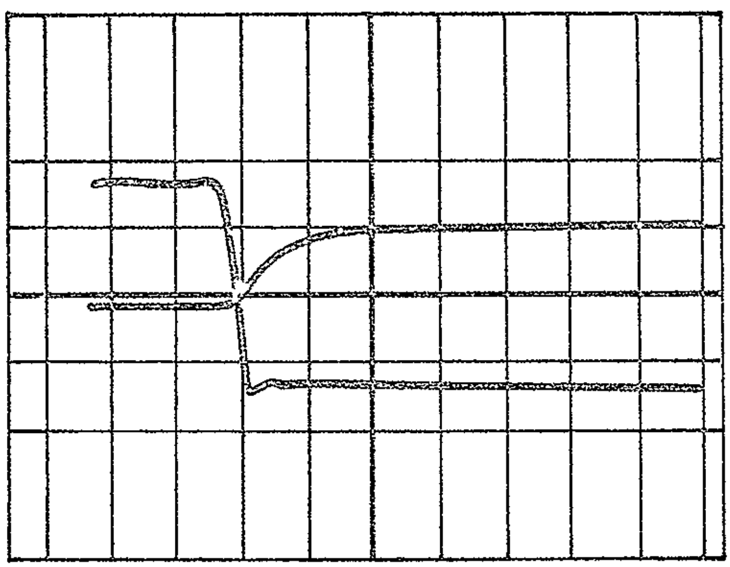

Input tail pulser

Output charge preamplifier with 100 pf input capacitance

50 n sec/div

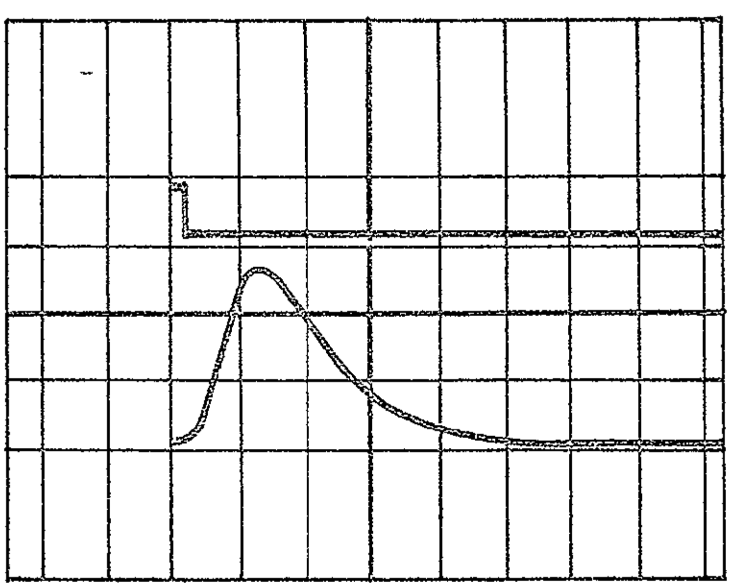

Input tail pulser

Output main pulse amplifier

1 μ sec/div

Test set-up for Detector Noise measurement

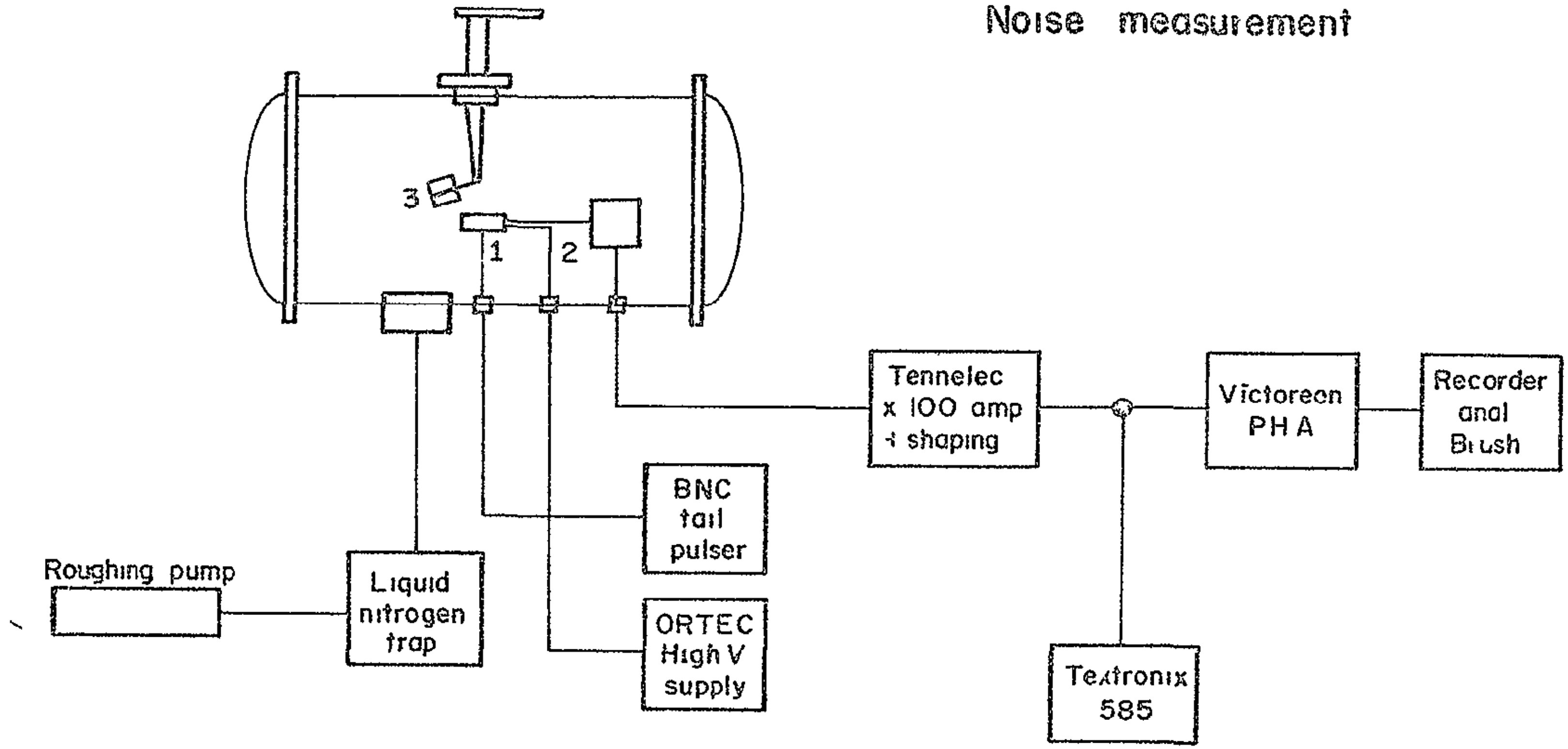

1 Detector with Field effect
and bias and feed b circuit

2 ampl x 100

3 Fe55 and I_{129} sources moveable

Figure 18

KEVEX 1193 LITHIUM DRIFT DETECTOR

-50°C 1 μ sec time constant

900V bias voltage

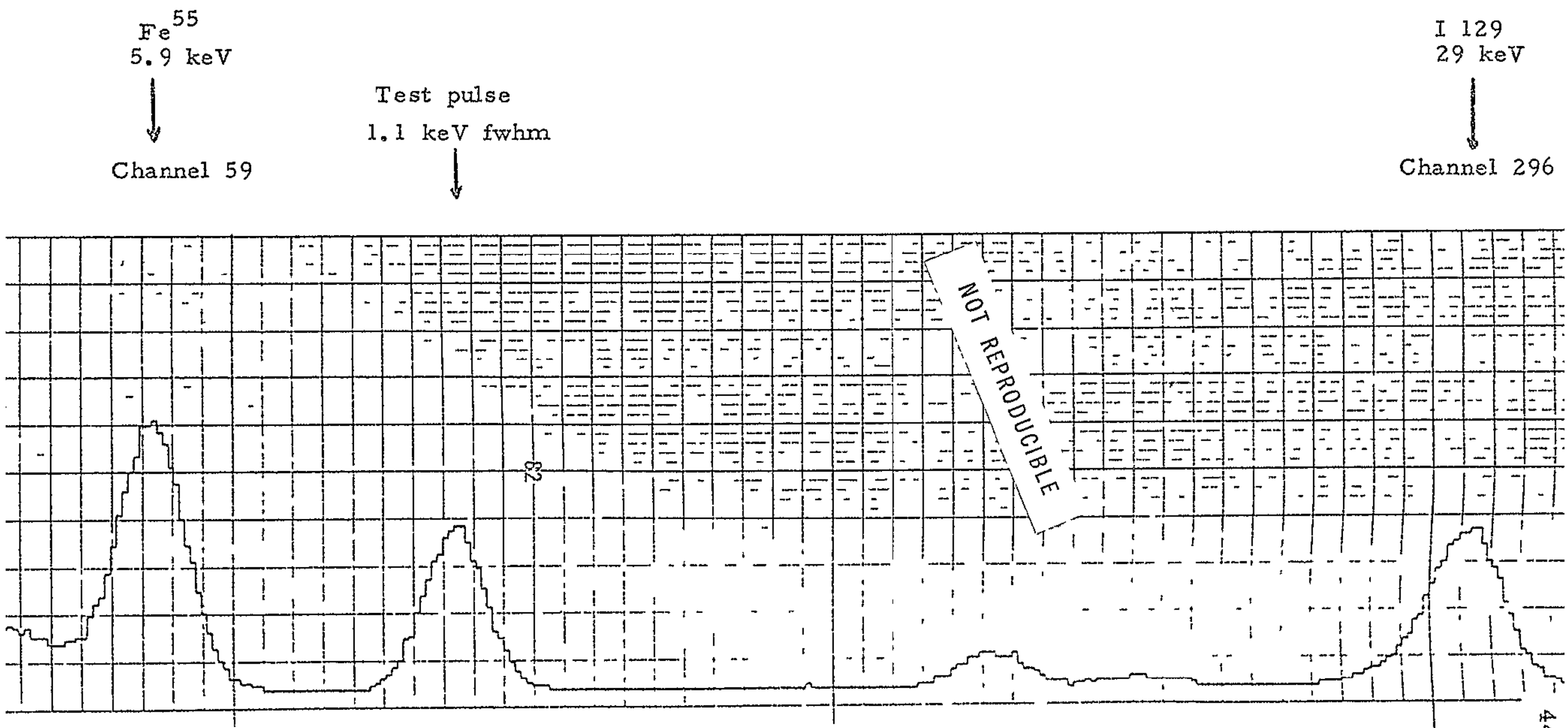

Figure 19

APPENDIX I

THE ELECTROSTATIC ANALYZER

A. Particle Trajectories

Each electrostatic analyzer used in the experiment can be represented by two concentric spherical conducting plates of radii R_1 and R_2 with an electric potential, V, applied between them, as shown in Figure A1a.

The motion of a charged particle between the plates can be determined by the force equation

$$\vec{F} = m \frac{d\vec{v}}{dt} \qquad (1)$$

where $\vec{F}$ is the force on the particle, m is the mass of the particle, $\vec{v}$ is the velocity of the particle and t represents time. If we consider only the electrical forces and use polar coordinates whose origin is at the center of the spheres the equation is written

$$e\vec{E} = m \frac{d}{dt} [\hat{r}\, \dot{r} + \hat{\varphi}\, r\, \dot{\varphi}] \qquad (2)$$

where e is the charge of the particle, $\vec{E}$ is the electric field, $\hat{r}$ is a unit vector in the radial direction, r is the distance from the origin to the particle, $\hat{\varphi}$ is a unit vector in the direction perpendicular to $\hat{r}$, φ is the angle between $\hat{r}$ and some fixed radius and the dot over a variable represents its derivative with respect to time. Taking the derivative of the right hand side of the equation as indicated we obtain

$$e\vec{E} = m [\hat{r}\, (r - r\dot{\varphi}^2) + \hat{\varphi}\, (r\varphi + 2\dot{r}\dot{\varphi})] . \qquad (3)$$

From the spherical symmetry of the problem we can determine that the electric field must be of the form

$$\vec{E} = -\hat{i}\,\frac{K}{r^2} \tag{4}$$

where K is a constant that can be determined from the difference in potential between the plates. Since

$$V = -\int_{R_1}^{R_2} \vec{E} \cdot d\vec{r} \tag{5}$$

then

$$K = V\left[\frac{1}{R_1} - \frac{1}{R_2}\right]^{-1} \tag{6}$$

where V is positive if the potential of the plate of radius R_2 is greater than the potential of the plate of radius R_1.

Since $\vec{E}$ is radially directed the last term in equation (3) must be zero. But this term is the time derivative of the angular momentum, L, of the particle which is given by the equation

$$L = mr^2\dot{\varphi} \tag{7}$$

thus the angular momentum is a constant.

The force equation (equation 1) can now be written

$$-\frac{eK}{r^2} = m(\ddot{r} - r\dot{\varphi}^2). \tag{8}$$

To obtain the equation of motion of the particle we must express equation (8) completely in terms of spatial coordinates. To do this we first note that

$$\dot{r} = \frac{dr}{d\varphi}\,\dot{\varphi} \; . \tag{9}$$

Taking the time derivative of this we obtain

$$r = \frac{d^2 r}{d\varphi}\,\varphi \; . \tag{10}$$

Since the time derivative of the angular momentum is zero, we may write

$$\varphi = -\frac{2\,\dot{r}\,\dot{\varphi}}{r} \tag{11}$$

and therefore

$$r = \left[\frac{d^2 r}{d\varphi^2} - \frac{2}{r}\left(\frac{dr^2}{d\varphi}\right)\right]\dot{\varphi}^2 \tag{12}$$

The coefficient is $\dot{\varphi}^2$ is a perfect differential, thus

$$r = -r^2\,\frac{d^2}{d\varphi^2}\left(\frac{1}{r}\right)\dot{\varphi}^2 \tag{13}$$

We use this expression in equation (8) to obtain

$$-\frac{eK}{r^2} = m\left[-r^2\,\frac{d^2}{d\varphi^2}\left(\frac{1}{r}\right) - r\right]\dot{\varphi}^2 \; . \tag{14}$$

Expressing $\dot{\varphi}^2$ in terms of the angular momentum and rearranging terms we have finally

$$\frac{d^2}{d\varphi^2}\left(\frac{1}{r}\right) + \frac{1}{r} = \frac{eKm}{L^2} \qquad (15)$$

The solution to equation (15) is of the form

$$\frac{1}{r} = P\ \cos\varphi + Q\ \sin\varphi + \frac{eKm}{L^2} \qquad (16)$$

The values of the constants P and Q must be determined from the initial conditions. For simplicity, we may choose the initial position of the particle to be $\varphi = 0$ and $r = r_o$ with the condition that

$$R_1 < r_o < R_2. \qquad (17)$$

The value of L is also an initial condition

$$L = mv_o\ \cos\theta\ r_o \qquad (18)$$

where v_o is the magnitude of the initial velocity of the particle and θ is the angle between the particle velocity and the tangent to the circle of radius r_o at the initial position, as shown in Figure A1a. We now introduce the parameter, a, such that

$$a = \frac{eK}{2T} \qquad (19)$$

where T is the kinetic energy of the particle

$$T = \tfrac{1}{2} m v_o^2 \tag{20}$$

This allows us to write equation (16) in terms of the initial values of r_o and θ

$$\frac{1}{r} = P \cos\varphi + Q \sin\varphi + \frac{a}{r_o^2 \cos^2\theta} \tag{21}$$

The condition that if $\varphi = 0$ then $r = r_o$ requires that

$$P = \frac{1}{r_o} - \frac{a}{r_o^2 \cos^2\theta} \tag{22}$$

The value of Q is determined from the derivative $dr/d\varphi$ at $\varphi = 0$. The particle is initially at $\varphi = 0$ and $r = r_o$, after traveling a short angular distance, $\Delta\varphi$, it has a new value of r, from Figure A1b.

$$r = \frac{r_o}{\cos\Delta\varphi} - r_o \tan\Delta\varphi \tan\theta . \tag{23}$$

The change in r is

$$\Delta r = r - r_o \tag{24}$$

If we consider only small values of $\Delta\varphi$ then

$$\Delta r = -r_o \Delta\varphi \tan\theta \tag{25}$$

Taking the limit as $\Delta\varphi \to 0$ we find that

$$\left.\frac{dr}{d\varphi}\right)_{\varphi = 0} = -r_o \tan\theta \quad . \tag{26}$$

This condition requires that

$$Q = \frac{1}{r_o} \tan\theta \tag{27}$$

The electrostatic analyzer is constructed of sections of hemispherical plates where particles enter on one side, travel through 180^o and exit on the other side as shown in Figure A1a. Thus we would like to know if a particle of known initial values of T, r_o and θ can make it around 180^o without colliding with one of the plates. To do this we first determine the values of $\varphi = \varphi_{ex}$ for which r reaches an extreme by setting

$$\frac{d}{d\varphi}\left(\frac{1}{r}\right) = 0 \tag{28}$$

This yields

$$\varphi_{ex} = \tan^{-1} \frac{Q}{P} \tag{29}$$

We are only interested in values of φ_{ex} such that

$$0^o \leq \varphi_{ex} \leq 180^o \quad . \tag{30}$$

To get the value of $r = r_{ex}$ at this point, put $\varphi = \varphi_{ex}$ into equation (21). For a particle to travel through 180^o it is required that

$$R_1 < r_{ex} < R_2 \tag{31}$$

If θ is initially negative then r_{ex} is a maximum and if θ is positive r_{ex} is a minimum. The opposite extreme value of $\dot{r}$ occurs at either $\varphi = 0^\circ$ or $\varphi = 180^\circ$ therefore we must also require that

$$R_1 < r_{180} < R_2 \tag{32}$$

where

$$r_{180} = -P + \frac{a}{r_o^2 \cos^2 \theta} \tag{33}$$

is the value of r when $\varphi = 180^\circ$. The above conditions along with the initial requirements on r_o (equation 17) guarantee that the particle will travel through the 180°. If a particle is deflected through 180° we say that it has an allowed trajectory.

Due to the spherical symmetry the above two-dimensional analysis is valid for all particle trajectories provided that the parameters r_o and θ are measured in the plane that includes the initial particle trajectory and the center of the spheres. Since the actual analyzer plates are only sections of hemispheres, as shown in Figure A1c, we must also require that the above plane be included within the wedge angle α and circumference section ℓ.

B. Geometry Factor

The geometry factor of the electrostatic analyzer can be defined by the equation

$$CR \left[\frac{\text{particles}}{\text{sec}}\right] = \int_T g(T) \left[\text{cm}^2 \cdot \text{sec}\right] j(T) \left[\frac{\text{particles}}{\text{cm}^2 \cdot \text{sr} \cdot \text{sec} \cdot \text{KeV}}\right] dT \left[\text{KeV}\right] \tag{34}$$

where CR is count rate or number of particles deflected through the analyzer, g(T) is the geometry factor for particles of energy T and j(T) dT is the flux of particles with kinetic energy between T and T + dT. Thus the geometry factor is an indication of the sensitive area and acceptance angle of the analyzer for particles of energy T. We can compute g(T) by the formula

$$g(T) = \int_A \int_\Omega dA\, d\Omega \tag{35}$$

where dA and dΩ are increments of area and solid angle and the integrals are carried out over those areas and solid angles for which particles of kinetic energy T have allowed trajectories.

We can rewrite the above equation in terms of the initial values θ, α, r_o and ℓ by substituting

$$d\Omega = d\alpha\, d\theta \tag{36}$$

and

$$dA = d\ell\, dr_o$$

then

$$g(T) = \int_\alpha \int_\theta \int_e \int_r d\alpha\, d\theta\, db\, dr_o \tag{38}$$

where the integrals are carried out over those initial values for which particles of energy T have allowed trajectories.

We can determine if a particle of energy T and initial values θ, α, r_o, and ℓ has an allowed trajectory by computing r_{ex} and r_{180} as explained in the preceding analysis. If r_{ex} and r_{180} satisfy the constraints $R_1 < r < R_2$ then the trajectory is allowed provided the plane of the trajectory is within the wedge angle α and circumference section ℓ.

To facilitate computation we introduce the function $f(\theta, \alpha, r_o, \ell, T)$ such that

$$f = \begin{cases} 1 & \text{if the trajectory is allowed} \\ 0 & \text{if the trajectory is not allowed} \end{cases} \tag{39}$$

then

$$g(T) = \int_{-\infty}^{\infty} \int_{-\infty}^{\infty} \int_{-\infty}^{\infty} \int_{-\infty}^{\infty} f(\theta, \alpha, r_o, \ell, T)\, d\theta\, d\alpha\, dr_o\, d\ell \tag{40}$$

This function was computed numerically for the analyzer configuration used in the experiments. The transmission matrix is the above function not integrated over α and θ giving $g'(T, \alpha, \theta)$. Due to spherical symmetry this function is the same for all values of α. g' is tabulated against T and θ to give the transmission matrix.

Since we normally do not know $j(T)$ we must assume that $j(T)$ is constant over the small interval of energy for which the analyzer is sensitive. Thus we assume

$$CR = j(T) \int_{0}^{\infty} g(T')\, dT' = G \cdot j(T) \tag{41}$$

where G is the total geometry factor and T is in the middle of the energy range for which the analyzer is sensitive. Since we measure CR and compute G we can determine j(T) by

$$j(T) = \frac{CR}{G} \tag{42}$$

In this case j(T) is the average flux over the small energy interval centered about T for which the analyzer is sensitive. By applying different voltages to the analyzer plates we can obtain many such averages. For the analyzers used in the experiment the energy interval was approximately 10% of the particle energy T.

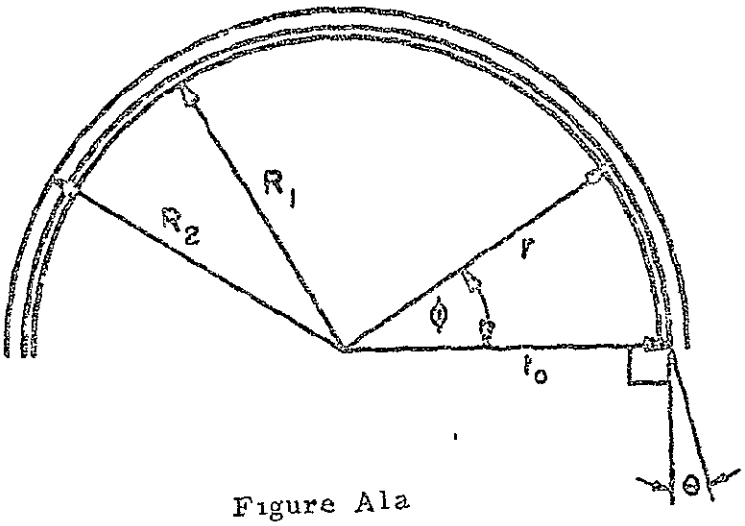

Figure A1a

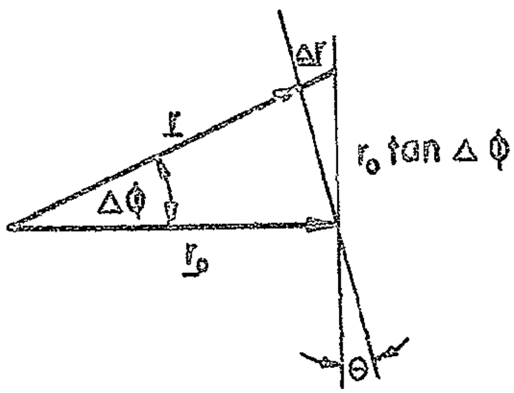

Figure A1b

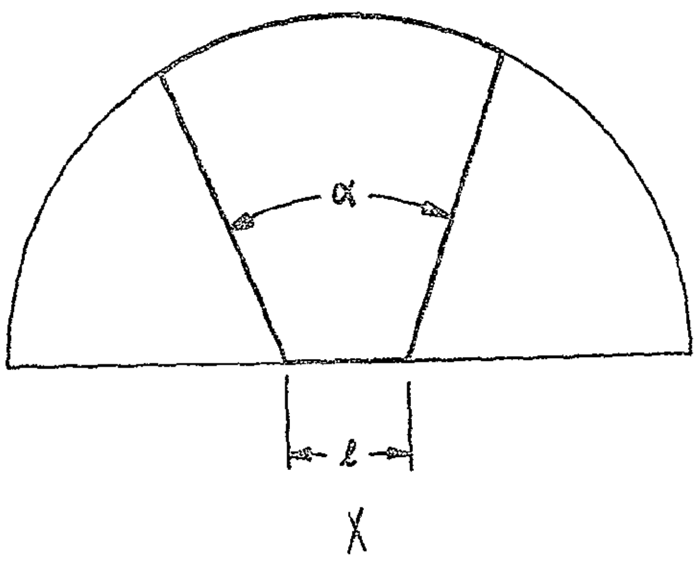

Figure A1c